In Vivo Multi-Day Calcium Imaging of CA1 Hippocampus in Freely Moving Rats Reveals a High Preponderance of Place Cells with Consistent Place Fields

Hannah S Wirtshafter[1*], John F Disterhoft[1]

*Lead contact: hsw@northwestern.edu (HSW)

1. Department of Neuroscience, Northwestern University Feinberg School of Medicine, Chicago, IL, USA.

Abstract

Calcium imaging using GCaMP indicators and miniature microscopes has been used to image cellular populations during long timescales and in different task phases, as well as to determine neuronal circuit topology and organization. Because the hippocampus (HPC) is essential for tasks of memory, spatial navigation, and learning, calcium imaging of large populations of HPC neurons can provide new insight on cell changes over time during these tasks. All reported HPC in vivo calcium imaging experiments have been done in mouse. However, rats have many behavioral and physiological experimental advantages over mice. In this paper, we present the first in vivo calcium imaging from CA1 hippocampus in freely moving rats. Using the UCLA Miniscope, we demonstrate that hundreds of cells can be visualized and held across weeks, and that calcium events in these cells are highly correlated with periods of movement. We show that an extremely large percent of cells recorded during recorded on a navigational task are place cells (77.3±5.0%, surpassing the percent seen during mouse calcium imaging), and that these cells enable accurate decoding of animal position and can be held over days in a consistent spatial map. A detailed protocol, including notes on the numerous parameter changes needed to use calcium imaging in rats, is included, and implications of these advancements are discussed.

Introduction

The explosion in the use of *in vivo* calcium imaging has allowed the visualization of hundreds of identified neurons over long time periods [1-8]. Calcium (Ca2+) imaging using GCaMP calcium indicators and miniature microscopes has been used to image cellular populations during long timescales [9-15] and in different task phases [16-18], as well as to determine neuronal circuit topography and organization [19-22].

The hippocampus (HPC) has been studied with cellular resolution using *in vivo* electrophysiology, but this technique does not allow the same cells to be definitively followed over days, nor does it allow the visualization of cellular organization within the structure [23-27]. *In vivo* calcium imaging is particularly well suited for imaging the rodent HPC, as the orientation of the horizontal cell layer permits imaging of large numbers of neurons with insertion of a 1mm diameter or smaller lens [12, 13, 22, 28]. Because the hippocampus is essential for many tasks involving memory [15, 29-37], spatial navigation [38-43], and learning [44-47], Ca2+ imaging of large populations of HPC neurons can shed new insight on cell changes and organization over time during these tasks.

To our knowledge, all reports of hippocampal *in vivo* calcium imaging have been done in mouse (although calcium imaging has been used to visualize other structures in rat [48-51]). Using calcium imaging in rat hippocampus requires optimizing a number of methodological parameters, including aspiration and lens implantation techniques, to account for the increased thickness of the rat alveus compared to mouse which makes focusing on the CA1 cell layer difficult [52-54]. However, rats have many basic experimental advantages over mice: First, rats are able to learn and perform more complex tasks than mice, and employ more advanced strategies, and are thus suited for a wider variety of behavioral experiments [55-60]. Second, compared to mouse physiology, rat physiology for a number of conditions and disorders (including addiction, aging, and schizophrenia, among others) more closely mirrors human physiology [61-64]. Third, rats are less stressed by handling than mice, thus introducing less variability in experimental procedures [65].

Rats are also an advantageous organism to use for calcium imaging: Due to their larger size, rats are able to support larger implants, including a wider diameter imaging lens, larger and heavier cameras that may be available in the future, and more combinations with electrophysiology implants. This advantage will thereby enable the recording of a greater number of cells [2, 66, 67]. Additionally, rat hippocampal neurons are less excitable than those in mice [54, 59], and rats are less prone to post-operative seizures than mice [68-70]. Rats may therefore, compared to mice, be at a decreased risk of the seizures (and potentially to cell death) seen in mice after prolonged GCaMP expression [5, 6, 71-73].

Although *in vivo* Ca2+ imaging would appear to hold substantial promise for the study of hippocampus in freely moving rats, there is currently no direct evidence that it will work in this system. To our knowledge, there are no published studies employing *in vivo* Ca2+ imaging in rat hippocampus, likely partially due to the number of methodological changes necessary to adapt the technique from mice to rats. In this paper, we present reports of *in vivo* Ca2+ recording from CA1 hippocampus in freely moving rats. We demonstrate that hundreds of cells are reliably visualized and held across weeks using this technique, and that calcium activity corresponds to periods of movement. We show that during a navigational task involving retrieving food reward on a linear track, a uniquely high percentage (77.3±5.0%) of imaged cells are place cells (as compared to calcium imaging studies in mouse and electrophysiology studies in rat and mouse), and that these place cells enable accurate decoding and can be held stably over days with little change in field location. A detailed protocol for this technique, including notes on the numerous parameter changes needed to use Ca2+ in rats, is included in the Materials and Methods section, and implications of these advancements are discussed.

Results

To initiate Ca2+ imaging, we injected AAV9-Syn-GCaMP7c below the CA1 cell layer in five male Fischer 344 x Brown Norway rats (Figure 1a, see Materials and

105 Methods) [74]. After injection, in the same surgery, cortex and corpus collosum were
106 aspirated through a craniotomy until the alveus was clearly visible (Figure 1b, see
107 Materials and Methods). A 2mm diameter GRIN lens was inserted into the craniotomy
108 and cemented in place. Three animals were checked for GCaMP expression four weeks
109 after surgery, and all three animals showed expression and were subsequently affixed
110 with a base plate to secure the position of the Miniscope. The other two animals were
111 checked six weeks after surgery and showed expression and were base plated. After
112 the completion of the experiment, animals were sacrificed and expression of GCaMP in
113 CA1 pyramidal cells was verified with microscopy (Figure 1c).
114 Animals were then food deprived to 85% body weight and trained on a 2.64m
115 linear track (Figure S1a). Animals were rewarded with grain pellets on alternating ends
116 of the linear track and quickly learned to run back and forth on the track (Figure S1b). A
117 visit to one reward well signified a trial. Animals were run for a minimum of 30 minutes
118 or 50 trials, whichever came later, with total track time not to exceed one hour per
119 session. Cells were recorded for 7 days for one animal, 11 days for one animal, and 16
120 days for two animals (n=4 rats, one of the five animals was eliminated when the implant
121 was lost).
122 The six sessions with the most trials run were analyzed from each animal
123 (average trials run = 100.3±33.1, see Materials and Methods), with first and last
124 recorded sessions automatically included; sessions were not always consecutive (see
125 Materials and Methods). These sessions were analyzed for cellular activity using the
126 CNMF-E method implemented by the CIATAH software package [75-77] (See Materials
127 and Methods). A total of 5761 neurons were recorded over the 24 sessions, with a
128 maximum of 428 cells from a single session (mean of 239.6±90.0 cells) (Figure 2a-d).
129 The number of cells recorded from each animal across sessions was relatively constant
130 (Figure 2c).
131 We then determined average calcium events/s across animals to be 0.090+-
132 0.019 events/s, with individual animals averaging 0.084+-0.024, 0.074+-0.026, 0.085+-
133 0.020, and 0.116+-0.032 events/second. (Figure 2D-E). There was a significant positive
134 correlation between the animal's average speed and the average events/s for each

135 session (F(22)=4.2, p=0.05) (Figure 2F). In every session, we saw a positive correlation
136 between the animal's speed and the number of calcium events across the population
137 (average correlation was 0.2 +-0.7 at an average lag of +4.7+-5.4s) (Figure 2G).
138 Significantly, calcium activity appeared to be heavily modulated by the animal's
139 activity, with periods of higher activity when the animal was running rather than
140 stationary on the track (Figure 3). The biggest contributor to a change in event rate was
141 transition from no movement to movement, with very few events occurring during
142 periods of no movement (Figure 3C).
143 We then determined if there were place cells on any of the trials. A cell was
144 considered to be a place cell if the mutual information (MI) computed in either direction
145 of travel was greater than 95% of MI scores computed 500 times after shuffling the
146 times of the calcium events that occur when the animal is moving [14, 78]. Based on
147 this criterion all trials contained place cells (Figure 3a). An average of 77.3±5.0%, of
148 cells were place cells (Figure 3), with individual rat averages at 71.6±10.6%, 77.3±1.2%,
149 76.4±9.5%, and 83.7±7.1%. We additionally determined the percentage of place cells if
150 we only analyzed cells that had an average calcium events rate of greater than 0.01hz
151 [28]. This additional criterion yielded an even higher percentage of place cells, with
152 88.3±4.4% of these cells being classified as place cells. (Figure 3a).
153 We extended these results using an additional criterion previously used to
154 determine the percentage of place cells using calcium imaging [28]. We determined the
155 percentage of cells that would be place cells if the mutual information value exceeded
156 the mean plus three standard deviations of a shuffled distribution. Using this criterion,
157 we found that 64.3+-5.1 percent of all cells were place cells, with individual animals at
158 59.5+-12.0%, 65.5+-2.3%, 61.2+-14%, and 71.0+-12.1%. If we applied the 0.01hz
159 threshold for cell inclusion to this group, 73.4+-4.3% of cells were place cells, with
160 individual animals at 68.0+-11.8%, 77.6+-5.6%, 77.0+-14.6% and 76.0+-13.0% (Figure
161 S2).
162 We wished to further investigate the properties of these place cells and to
163 confirm that cells were increasing their firing rate in place fields as is typical for
164 pyramidal cells; as opposed to interneurons that mark spatial location by a substantial

decrease in firing [11, 79, 80]). We examined the place cells' maximum event rate during movement (presumably occurring in the place field) with their average firing rate during movement. The mean maximum rate was 0.15events/s, and the mean average rate was 0.02events/s. On average, cells increased firing 7.4x from their average firing rate during movement to their maximum firing rate (Figure 4D).

We then aimed to determine whether place cell firing was sufficient to decode the position of the animal. We split the track in 10cm segments and used Bayesian decoding to determine the position of the animal in non-overlapping 0.5 second increments [81]. We found that the best positional decoding was accurate to a median error of 4.3cm (1.6% of the 2.64m track). Across all animals, accuracy ranged from a median of 4.3cm to 13.6cm (decoding errors were below 10cm in 23 sessions and above 10cm in one session) with a median error of 5.9cm (Figure 5a). To confirm that decoding accuracy was better than chance we shuffled firing rate per position bins and, using the shuffled data, decoded position. Median error for shuffled data ranged from 59.1cm to 77.6cm, which was significantly worse than non-shuffled data (Kruskal-Wallis test, $x^2(47)= 35.3$, $p=2.9*10^{-9}$) (Figure 5b).

We then aimed to determine if the same cells could be held over the duration of our recordings (six recording sessions, spanning 7, 11, or 16 days). 40% of the cells imaged on day one of the 7-day session were also present on day seven. Of the rat run for 11 days, 31% of the cells present on day one were also present on day eleven. For the two rats run 16 days, 28% and 50% of cells, respectively, that were present on day one were also present on day sixteen. Across all four animals, cells that were imaged on day one of recording had, on average, a 72±6% chance of being imaged on at least one subsequent day of recording (Figure 6A). (Of note, while the camera was placed in the same approximate position each day, the focal plane was not always held constant and recordings each day were made to optimize total cell number in each day as proof of method, rather than to maintain the same landmarks or focal planes.)

We then looked to determine how often a cell appeared in each session. Across all cells, 59.4+-5.4% of cells were visible in only one session, 19.9+-2.4 were visible in two, 11.2+-1.5 in three, 6.3+-0.8 in four, 2.3+-1.3 in five, and 1.0+-0.9 were in all six

195 sessions (Figure 6B). We then looked at place cells that were repeated across
196 sessions. As stated, 22.6+-4.3% of cells did not have place cells in any session. Of the
197 77.4% of cells that did have place fields, 61.0+-5.7% (47.2% of total cells) had fields in
198 only one session, 20.6+-2.0 (15.9% of total) had fields in two sessions, 10.8+-2.4%
199 (8.3% of total) had fields in three sessions, 5.1+-0.7% (4.9% of total) had fields in four
200 sessions, 2.0+-1.4% (1.5% of total) had fields in five sessions, and 0.5+-0.5 (0.4%of
201 total) had fields in all six sessions (Figure 6C). Place cell recurrence was not statistically
202 different from the recurrence of all cells (paired t-test(5)=$2.04*10^{-15}$, p=1).
203 We then determined the recurrence probability of a cell based on the number of
204 days apart the recording took place (Figure 6D). Three of our animals had relatively
205 consistent recurrence probabilities, while one animal (animal 3) was highly variable.
206 Going back to the recordings, we saw that recordings from this animal came from two
207 different focal planes, causing the recording of two different cell populations. Excluding
208 this animal, there was a modest trend across days for a decreasing recurrence
209 probability, with the probability of a cell reoccurring decreasing by 0.43% per day
210 separating the recording periods (Figure 6E).
211 We then determined whether a cell's place field remained in the same location
212 during days when the place cell reoccurred. We found that, across all days of recording,
213 the mean standard deviation of place field locations was about 36cm (~13% of track
214 length), with the individual animals at 39cm, 36cm, 32cm, and 37cm. We compared
215 these distances with distances if place field locations were shuffled, and we repeated
216 shuffling 500 times. All four animals had a smaller deviation between fields than would
217 be expected by chance ($p<0.05$ for all animals). Between individual days (including
218 nonadjacent days), the change in field distance was highly variable at 65cm+-71cm,
219 with a median of 40cm and a large concentration of values around 0cm (Figure 6F).
220 Although fields across days were more consistent than would have been
221 expected by random chance, we had not yet determined whether the animal had a
222 consistent map across all recording days [14], or if it switched between multiple maps
223 [13]. To determine this, we compared place field location for cells in a session against
224 the place field locations of the same cells in another session. Of the pairs of sessions

that had more than 10 place cells shared between sessions (57 out of 60 total session pairs—15 session pairs for rat 1, 15 for rat 2, 14 for rat 3, and 13 for rat 4), 53 of these pairs (93%) had a significant positive correlation between the place field locations in both sessions, with no evidence of switching between maps across days (Figure 6G). We found that correlations between field locations did not decay as a function of the number of days between sessions (Figure 6HG).

Discussion

In this manuscript, we have demonstrated calcium imaging recordings can be performed in the CA1 region of the hippocampus in freely moving rats. These recordings can capture hundreds of cells in a single recording session, including a high number and percentage of place cells sufficient to decode the animal's position to within centimeters of accuracy, and that place cell field location is consistent across days. Calcium imaging in rat will allow for more behaviorally complex and translational experiments than have been done in mouse.

We chose to use mutual information as the measure of spatial content for multiple reasons: First, it has precedence for use in both calcium imaging [12, 14, 28, 78, 82] and electrophysiology studies [83] (Table 1). Second, threshold measures commonly used in electrophysiology that depend on firing rate (such as "a cell is a place cell if firing rate, as measured by electrophysiology, exceeds 2Hz for a 10cm area") [84] (Table 1) do not transfer well to calcium imaging experiments as, using currently availably GCaMPs, calcium events are captured much less frequently than spikes in electrophysiology [28]. Third, other measures of information content, such as bits/spike or bits/second (Table 1), tend to be highly sensitive to changes in firing rate, including baseline firing rate [85], as compared to mutual information. Specifically, cells with lower baseline firing rates are favored to have higher baseline bits/spike or bits/second values [85, 86], which makes it not a useful metric with which to compare values from calcium imaging with data collected from electrophysiology. Additionally, mutual information is

255 advantageous in that it is a better predictor of decoding accuracy than bits/spike and
256 bits/second, and thus may better capture spatial informational content [85]. The criteria
257 we used to identify place cells were as or more stringent than previously used criteria in
258 calcium imaging that identified a significantly lower percentage of place fields (Table 1).
259 Significantly, we found a higher percentage of cells were place cells in our
260 calcium imaging experiments in rats than those reported in mouse CA1 calcium imaging
261 experiments, even after the mice experiments were corrected for cells with low spiking
262 rates (Table 1). (The studies with mice reported 20-30% of imaged CA1 cells were
263 place cells, which is also substantially below most electrophysiology experiments [14,
264 87]). Previous work has reported that mouse place cells are less spatially tuned, contain
265 less spatial information, and have less stable place fields than in rat [59, 88], so some of
266 the difference in place cell percent may be due to species differences in spatial
267 representations. However, there are also likely physiological differences between rats
268 and mice that affect the type of activity captured in calcium imaging recordings. CA1
269 cells in mice are more excitable than those in rat [54, 59], and prolonged GCaMP
270 expression in mice has been shown to lead to cell hyperexcitability, seizures, and even
271 cell death [5, 6, 71-73]. The higher baseline excitability of mouse cells, combined with a
272 further increase in cellular excitability after GCaMP expression may result in a lower
273 threshold for cell firing and less defined place fields, less stable fields, and, therefore, a
274 seemingly lower number of place cells compared to electrophysiology recordings [59].
275 Because rats have a lower baseline excitability, they may be less prone to these
276 GCaMP effects, although further slice electrophysiology work will need to be done to
277 directly compare the effect of GCaMP on mouse and rat neurons.
278 In addition to potentially allowing the recording of a higher number of place cells,
279 the lower excitability of rat CA1 neurons, compared to mouse, also has other
280 advantages. We saw no behavioral evidence of post-operative seizures in any of our
281 implanted animals, and no behavioral or imaging evidence of seizures several months
282 post viral injection and lens implementation. This is in contrast to calcium imaging
283 experiments in mice, which frequently report that animals have to be removed from
284 behavior or analysis due to the development of seizure activity [71, 89].

285

286 The percentage of hippocampal CA1 cells found to be place cells using calcium
287 recordings (77.3+-5.0%) was also very slightly above the upper range of findings from
288 electrophysiological data in rats, which report that 35-75% of CA1 pyramidal cells
289 recorded on a navigational task are place cells (the number varies widely depending on
290 task parameters, with studies using a linear track task reporting the highest number of
291 place cells) (Table 1) [86, 90, 91]. There are multiple possible reasons related to
292 recording technology as to why our calcium imaging experiments detected a higher
293 percentage of place cells than traditional electrophysiology experiments: the difference
294 likely resulted from electrophysiology capturing (as compared to calcium imaging) both
295 a lower number of cells with active place fields detected (a smaller numerator) and a
296 larger number of cells without active place fields detected (a larger denominator). First,
297 in electrophysiology experiments with moveable electrodes (such as tetrodes),
298 electrodes are typically positioned while rats are inside a “sleep box” or other non-
299 training apparatus until cells are detected. The animal is then placed on a track for
300 experimentation. This practice optimizes cell detection for place cells that are active in
301 the “sleep box” (both place cells with fields in the sleep box, and place cells that are
302 reactivated during ripples during sleep), rather than cells that have place fields on the
303 track. Adjusting and recording in a sleep box therefore increases the number of total
304 cells recorded that do not have fields on the track and therefore reduce the place cell
305 percentage. Because calcium imaging uses a fixed lens location and images a large
306 number of cells at once, recording is not optimized for a particular environment. This
307 may result in the recording of a higher percentage of active place cells on the recording
308 apparatus. Additionally, in this study, we did not complete any recording while the
309 animal was not on the track, thereby decreasing the number of cells recorded without
310 fields on the track. Second, while an effort is made in electrophysiology to discard times
311 on the track when the animal is not moving, and thus to remove corresponding spiking
312 during ripples, this removal is never perfectly done. The recording of ripples during
313 electrophysiology has two effects: the recording of cells that are being replayed on the
314 track but do not have place fields on the track and, second, the recording of ‘extra-field’

315 ripple spiking from cells with fields on the track. This ‘extra-field’ spiking can cause
316 place fields to seem less defined, and cause corresponding distortion of measures of
317 spatial information, such as mutual information and bits/spike. This, in turn, may cause
318 these cells not to be classified as place cells. Conversely, in calcium imaging, very few
319 to no calcium events are picked up during periods of no movement (see later in
320 discussion, figure 3), so both of these issues (increasing the count of cells without fields
321 on the track, and the distortion of spatial information for place cells) are avoided. Third,
322 while current GCaMPs, such as the GCaMP7c used in this study, have improved single
323 spike resolution compared to past GCaMPs, they still fall short of the single spike
324 resolution of electrophysiology [92-96]. This property of calcium indicators causes
325 individual spikes, such as those that may occur on the track outside a cell’s place field,
326 to be missed, therefore biasing calcium imaging towards fast cell activity that only
327 occurs in the confines of a place field. Calcium imaging therefore, again, results in
328 potentially higher spatial information metrics as compared to electrophysiology, which
329 may cause the identification of more place cells. Finally, compared to electrophysiology,
330 calcium imaging provides additional characteristics (cell shape, size, and brightness) by
331 which to separate adjacent or nearby cells. Because conflation of multiple cells may
332 disguise place fields and disrupt place field measurements (such as mutual information
333 or bits per spike) in electrophysiology, the additional resolution afforded by calcium
334 imaging may allow for more accurate place cell differentiation and identification.
335 Similar to electrophysiology and in contrast to intermediate early gene (IEG)
336 studies, calcium imaging is biased towards capturing cells active in an environment and
337 not the total cellular population. Additionally, as discussed above, due to limits on single
338 spike resolution, calcium imaging may be picking up even fewer cells with infrequent
339 spiking compared to electrophysiology. Thus, this bias of calcium imaging toward
340 detecting only active cells yields a higher percentage of place cells than intermediate
341 early gene studies that estimate a total of 30-40% of cells to be active in any given
342 environment (table 1) [97, 98].
343 We considered that differences in calcium event rate between our data and other
344 studies might lead to the high percentage of place cells we saw in this work. On one

end of the spectrum, Stefanini et al 2020 found a particularly low percentage of place cells (~4% of recorded cells in mouse CA1, using calcium imaging) and investigated whether this might be a consequence of collecting many cells with low calcium event rates. Their reported mean rate was 0.06+-0.04 events/s as recorded in mice in an open field, consistent with 0.05-0.5 events/s in other calcium imaging experiments in mouse. Even after eliminating cells with <0.1events/sec (a 10x less stringent criteria than we used in Figure 3A), they still only found that 10-20% of cells were place cells ([28]). Conversely, Ziv 2013, who reported a high (for mouse) 20% of imaged CA1 mouse cells were place cells, reported a higher mean event rate, at ~0.1-0.5 events/s [14]. Our results (0.090+-0.019 events/s, Figure 2D-E) are on the lower end of those reported in Ziv et al, and potentially consistent with the fact that rat neurons are somewhat less excitable than those in mice [54, 59]. Additionally, our very slightly lower event rate could be the result of less 'out of field' firing of place cells, which also tends to be more predominant in mice [59]. However, our results are within the range of those reported in mouse imaging studies, so differences in event rate are not a likely to be a major contributor to the place cell percentage we observed.

During our recording sessions, we saw clear evidence that calcium event rate was correlated with periods of movement (Figure 3). In electrophysiology experiments, place cell spiking is generally linearly correlated with running speed [99], and significant spiking occurs during ripples when the animal is not moving [100-103]. Our finding greatly differs from the patterns of spiking seen in electrophysiology data, as we saw minimal calcium events during periods of no movement, with a pattern of logarithmic growth of the number of calcium events as the animal began moving and sped up (Figure 3C). Our result is consistent with calcium imaging experiments done in mice by Zhou et al., in which more calcium events were seen during movement in an environment where food reward could be obtained than during quiet wakefulness in a neutral box [8]. In our experiment, periods of quiet wake were in the same environment (the track) as periods of movement, which shows that changes in calcium event frequency are related to movement and not to contextual associations. Zhou et al. posit that the high amount of calcium activity that occurs during movement, but not during

375 sharp wave ripples in mouse, implicate calcium events in theta dependent processes,
376 such as memory encoding and planning [104-110]. Given that AMPA receptor
377 antagonists abolish ripples in slice, while NMDA receptor agonists do not, it is possible
378 that NMDA receptors, which permit calcium influx, are minimally involved in cell spiking
379 during ripples [111, 112]. This would result in a smaller influx of calcium into the cell
380 during ripples compared to place field spiking and, thus, a smaller, less perceptible
381 signal during calcium imaging. Further work will be needed to determine if, in rat,
382 frequent calcium events are also unique to movement, as opposed to sharp wave
383 ripples.

384 Our findings on cell activity over days were similar to and consistent with prior
385 results reported in mice. Prior work has reported that about 57% of cells are active in
386 only one or two sessions [14]; we found a higher proportion (59.4+-5.4% of cells were
387 visible in only one session, 19.9+-2.4 were visible in two) (Figure 6B), likely because we
388 worked to optimize cell count over precisely consistent focal planes. We also reported
389 that probability of a cell reoccurring decreased by 0.43% per day separating recording
390 sessions. This result was exactly consistent with prior results in mouse that cell
391 reoccurrence decreases from ~25% for sessions 5 days apart to ~15% for sessions 30
392 days apart (25 days difference * 0.43 = ~10.8% change)(Figure 6E) [14]. This potential
393 cell turnover did not impact the accuracy of the representation of the environment, as
394 decoding accuracy was consistent throughout sessions [113].

395 There are differing results regarding whether an environment has a single semi-
396 stable map [1, 4, 5], or there are multiple maps, involving the same cells, that code for a
397 single environment [2]. In this study, we only saw evidence of the former, as the vast
398 majority of sessions had cells with place fields correlated to previous sessions (Figure
399 6F) and place field locations did not change as a function of the number of days
400 between sessions (Figure 6G). In other words, cell reoccurrence decreases across
401 days, but apparently when a cell does reoccur, its place field remains largely the same.

402 As previously mentioned, similarities between rat and human physiology, as well
403 as the increased capacity for complex tasks of learning and memory [55-60], position
404 rats as a well-suited model organism for studying hippocampal function, with several

advantages over the mouse. Rats are advantageous over mice in that, for many diseases and disorders, including those with substantial hippocampal involvement, their physiology and behavior more closely mirrors that of humans [63]. For instance, 5-HT serotonin receptors, which are prominent in the hippocampus and are implicated in a variety of disorders (including mood and anxiety disorders, psychiatric disorders such as schizophrenia, addiction and ADHD), are distributed in rats, but not in mice, in a similar pattern as seen in humans [63, 115]. Hippocampal neurogenesis, which is believed to play an important role in learning, memory, and the treatment of depression, is believed to follow a similar pattern in rats and humans, and is less pronounced in mice [116]. In addition, both pharmacologic and behavioral responses to addiction are more similar between rats and humans than mice and humans [63, 117, 118].

Having the ability to do calcium imaging in rat CA1 will allow increased research into these disorders, as well as basic research in learning and memory. Because rats are substantially larger than mice, they can support larger lens implants and cameras, which may lead to the ability to record from thousands of hippocampal cells in a single session during complex tasks. The ability to record a large number of cells across days will allow research into cell firing changes in the hippocampus, which will provide insight into more advanced learning and disease mechanisms that are difficult to understand when only investigating mice. Additionally, the uniquely high percentage of recorded place cells (>80% of recorded cells) makes CA1 calcium imaging in rats an ideal method by which to study spatial navigation and learning over days, including mechanisms behind memory consolidation, spatial remapping, and planning over time.

431 **Materials and Methods**

432

433 ***SUBJECT DETAILS***

434 All procedures were performed within Northwestern Institutional Animal Care and
435 Use Committee and NIH guidelines. Five male Fischer 344 x Brown Norway rats (275g
436 to 325g) were sourced from National Institute on Aging colony at Charles River
437 Laboratories, injected with AAV9-GCaMP7c, implanted with a 2mm GRIN lens and run
438 on linear maze (Figure S1). Animals were individually housed in an animal facility with a
439 12h light dark cycle.

440 ***METHOD DETAILS***

441 **GCaMP7s Injection and Lens Implantation**

442 Rats were anesthetized with isoflurane (induction 4%, maintenance 1-2%).
443 Following anesthesia, ear bars, and skull leveling, the skull was cleaned and a
444 craniotomy site was marked above CA1 (stereotaxic coordinates Bregma AP -4.00mm,
445 ML 3.00mm). The skull was scored around the craniotomy site using a razor blade to
446 provide texture for future application of epoxy. A craniotomy was made with a 2mm
447 trephine around the marked site and dura was removed with a bent 30 gage needle. A
448 Hamilton syringe (Gastight® 1700 Series Syringes, Hamilton, Model 1705 Small RN
449 Syringe, Volume=50 μL, Point Style=3, Gauge=22s, Needle Length=50.8 mm) loaded
450 with AAV9-GCaMP7c (obtained from Viogene Biosciences, packaged AAV9 of pGP-
451 AAV-syn-jGCaMP7c-WPRE, titer $1.73*10^{13}$GC/mL) was lowered straight down to about
452 0.2mm past the CA1 cell layer (approximate coordinates Bregma AP -4.00mm, ML
453 3mm, DV 2.95mm relative to skull). 0.6uL of virus were injected over 12 minutes using
454 an automated stereotaxic Injector. The syringe was then raised 0.2mm (Bregma AP -
455 4.00mm, ML 3mm, DV 2.75mm) and another 0.6uL of virus were injected over 12
456 minutes (Figure 1a). The syringe was then left for 10 minutes before slowly raising to
457 the skull.

458 We used a computerized stereotaxic injection system that allowed us to specify
459 the coordinates of the injection. Due to the imprecision of craniotomies and imperfectly
460 level skulls, often the initial injection at the specified sub-cortical coordinates did not fall

461 in the center of the craniotomy. To increase and maximize the spread of viral injection,
462 we completed a second injection. The process of lowering the syringe and doing two
463 injections was repeated so that the two syringe “lowering points” were evenly spread
464 throughout the craniotomy site. There were thus a total of four injections of 0.6uL each
465 (2.4uL total): two injections per each brain entrance site, each at different depths
466 (Figure 1a).

467 Following injection, four skull screws were screwed into the skull: one rostral to
468 bregma above the same hemisphere as the craniotomy, two between bregma and
469 lambda on the hemisphere opposite the craniotomy, and one behind lambda on the
470 hemisphere with the craniotomy. Under a dissecting microscope, tissue from the
471 craniotomy was then aspirated using a vacuum pump and 25 gage needle that had
472 been previously blunted using a Dremel drill. Tissue was quickly aspirated until the start
473 of horizontal striations could be seen in the craniotomy hole. Care was then taken to
474 “level” the hole and make sure aspiration was at an even depth. The horizontal
475 striations of the corpus callosum were then carefully and slowly aspirated until the
476 vertical striations of the alveus were visible in the entirety of the craniotomy hole (Figure
477 1b). If the aspiration hole was bleeding, a small twisted piece of gel foam was inserted
478 into the hole for approximately five minutes and then removed.

479 *Notes differentiating this method from mouse Ca2+ imaging: We found the best*
480 *AAV for expression in rats was AAV9. Because of rat’s lower seizure threshold and,*
481 *anecdotally noted, lower GCaMP expression than in mice, four injection sites appear*
482 *both necessary and sufficient for ideal GCaMP expression. The injection volumes are*
483 *much larger than those used in mice [14, 15], which is made possible due to the larger*
484 *hippocampal area and the technique of injecting below the CA1 cell layer, instead of on*
485 *it. Unlike in mice, where just the cortex or most dorsal part of the corpus callosum is*
486 *aspirated [15, 119], it is important that the entire corpus callosum be completely*
487 *aspirated in order to get very close to the alveus.*

488 A 2mm GRIN lens (obtained from Go!Foton, CLH lens, 2.00mm diameter, 0.448
489 pitch, working distance 0.30mm, 550nm wavelength) was then held on the end of a
490 pipette using suction from the vacuum pump. The pipette was placed in the stereotaxic

491 instrument which was zero-ed with the bottom of the lens on bregma. The lens was then
492 moved to the center of the craniotomy and lowered to a depth of approximately 3mm
493 from skull surface. The lens was then fixed in place with UV curing epoxy and the
494 vacuum pump was turned off and the pipette holding the lens removed. The epoxied
495 lens was then secured to the skull screws using dental acrylic. Animals were then given
496 buprenorphine (0.05mg/kg) and 20mL saline, taken off anesthesia, and allowed to
497 recover in a clean cage place upon a heat pad.

498 *Notes differentiating this method from mouse Ca2+ imaging: A much larger lens*
499 *(2mm diameter as opposed to 0.5mm or 1.0mm diameter) lens can be used in rats due*
500 *to their larger size. Of high importance: in order to be as close to the CA1 layer as*
501 *possible, the lens is inserted further down (about .5mm) lower than the cell layer. This*
502 *serves, presumably, to temporarily compress the alveus to make sure the alveus is*
503 *pressed against the grin lens; this allows for in focus imaging of the CA1. We saw no*
504 *permanent compression of the CA1 cell layer (Figure 1C) or any behavioral deficits that*
505 *are associated with HPC compression [120, 121]. We had zero visualization of cells*
506 *unless the lens was deeply inserted. Additionally, unlike in mouse implantation*
507 *surgeries, we did not have success using meloxicam after surgery as it appeared to*
508 *cause excessive bleeding around the lens.*

509 Four to six weeks after surgery, animals were again anesthetized with isoflurane
510 and checked for cells expressing GCaMP. If expression was seen, the animal's lens
511 was base-plated. The baseplate was attached using UV-curing epoxy and dental
512 acrylic.

513 *Notes differentiating this method from mouse Ca2+ imaging: During base plating,*
514 *it gets progressively harder to see cells the longer the animal is under anesthesia.*
515 *Additionally, while a few cells will appear to be bright circles in the captured image, cells*
516 *do not appear to be flashing at all while the rat is under isoflurane, even after a tail pinch*
517 *or loud noise (techniques often used to incite a calcium during mouse base plating). We*
518 *recommend focusing on the bright, not flashing cells while base plating. The entire field*
519 *of view should become progressively brighter as the animal wakes up. We recommend*
520 *not imaging for experiments within 24 hours of isoflurane exposure and base plating.*

521

522 **Behavioral Training**

523 Prior to training, animals were food deprived to 85% body weight and maintained
524 at this weight throughout the experiment. Implanted animals were trained on a 2.64m
525 Med Associates linear track with pellet dispensers at either end. Animals learned to run
526 back and forth between the sides of the track and received a grain pellet at alternate
527 ends. Each pellet received was considered a trial. The fasted animals were able to
528 achieve over 120 trials in 30 minutes. (Animal were fed after daily training to maintain
529 weight.) Six sessions were selected for analysis for each animal, with first and last
530 recorded sessions automatically included. When not being run, animals were housed in
531 individual cages with a 12hr light- 12hr dark light cycle.

532 Six sessions from each animal were selection for analysis. Although each animal
533 was run for at least seven sessions, occasionally an animal would refuse to run or run
534 slowly (often the day following a run with a lot of pellets received). For the animal run
535 the least number of times, only six sessions exceeded 50 trials per run. For consistency
536 across analysis, we therefore selected the six sessions with the most trials to analyze
537 from each animal. On average, the four animals ran 100.3+-33.1 trials per session, with
538 the individual animals averaging 94.7+-35.3, 85.5+24.0, 114.5+-19.8, and 106.2+-41.2
539 trials per session.

540 Because the runs with the most trials were selected for analysis, trials were not
541 always consecutive. If the first analyzed session is considered day 1, the analyzed
542 sessions were as follows for each animal (as numbered by days on a calendar; animals
543 were not necessarily run every day due to scheduling and equipment troubleshooting):

544 *Animal 1:* Days 1, 2, 3, 7, 8, 9 *(run across 9 days)*

545 *Animal 2:* Days 1, 2, 6, 7, 9, 13 *(run across 13 days)*

546 *Animal 3:* Days: 1, 2, 11, 14, 15, 16 *(run across 16 days)*

547 *Animal 4:* Days: 1, 2, 10, 14, 15, 16 *(run across 16 days)*

548

549 **Calcium Imaging**

One photon calcium imaging was done using UCLA V4 Miniscopes [122, 123], assembled with standard lens configurations (two 3mm diameter, 6mm FL achromat lens used in the objective module and one 4 mm diameter, 10mm FL achromat lens used in the emission module). We tested Ca2+ recording when one of the objective module lenses was replaced by a 3mm diameter, 9mm FL achromat lens, but no improvement in cell visualization was noted. Gain was set at high and Miniscope LED intensity varied between 10 and 38.

Notes differentiating this method from mouse Ca2+ imaging: Base fluorescence appears lower in rats as compared to mice. While we have been advised that, using Miniscopes, gain can often be on "low" for mouse imaging, we found it necessary to have gain on "high" to visualize the highest number of cells.

GCaMP Visualization in Slice

Following conclusion of the study, animals were anesthetized and perfused with PBS then 10% formalin. The brain was then sliced into 60 micron coronal sections, mounted, let dry, and coverslipped with Vectashield. Sections were then imaged with a confocal microscope.

QUANTIFICATION AND STATISTICAL ANALYSIS

Means are expressed as mean ± the standard deviation. Overall averages are computed by finding average per animal then averaging those values. All analysis code is available at https://github.com/hsw28/ca_imaging.

Position and speed analysis

Position was sampled by an overhead camera at 30Hz. Position tracking was done post-recording using Bonsai [124]. Speed was determined by taking the hypotenuse of the coordinates of the point one before and one after the time point of interest. Speed was then smoothed using a Gaussian kernel of 1s and speed was converted from pixels/s to cm/s.

580

581 **Video pre-processing**

582 Videos were recorded with Miniscope software at 15 frames/second and 752 by
583 480 pixels. All video processing was done using the Matlab-based CIATAH software
584 [76, 77] and processing files are available at https://github.com/hsw28/ca_imaging/ .
585 Videos were down sampled in space (3x using bi-linear interpolation) and time (2x). The
586 video was normalized by subtracting the mean value of each frame from the frame.
587 Each frame was then spatially filtered (normalized) using a bandpass FFT filter (70-
588 100cycles/pixel). The video was then motion corrected to a chosen reference frame
589 using TurboReg [125]. Videos were then converted to relative florescence (dF/F_0),
590 where F_0 was the mean over the entire video.

591

592 **Cell identification**

593 Cells were first automatically identified using the Matlab-based CIATAH software
594 [76, 77], using the CNMF-E method [75]. Processing files are available at
595 https://github.com/hsw28/ca_imaging/ . Images were filtered with a gaussian kernel of
596 width 3 pixels. Neuron diameter was set at a pixel size of 13. The threshold for merging
597 neurons was set at a calcium trace correlation of 0.65, and neurons were merged if their
598 distances were smaller than 2 pixels and they had highly correlated spatial shapes
599 (correlation>0.8) and small temporal correlations (correlation <0.4).

600 All cells identified using CNMF-E were then scored as neurons or not by a
601 human scorer. Scoring was also done within the Matlab-based CIATAH software [76,
602 77] in a Matlab GUI. Human scoring was done while visualizing an activity trace,
603 average Ca2+ waveform, a cropped movie montage of the candidate cell's Ca2+
604 events, and a maximum projection of all cells on which the candidate cell was
605 highlighted. The relative fluorescence ($\Delta F/F_0$) local maxima of each identified cell were
606 considered calcium event times.

607

608 **Place cell identification**

Place cells were identified using two criteria. First, cells must have a mean firing rate greater than 0.01Hz during periods of movement (>12cm/s) [86, 126]. Second, the mutual information (MI) computed in either direction of travel must be greater than 95% of MI scores computed 500 times from shuffled cells [78]. To compute MI, the track was divided lengthwise into 4cm bins the firing rate of each cell and the occupancy of the animal were found for each bin. Rate and occupancy were smoothed with a 2cm Gaussian kernel. Mutual information was computed during periods of movement in each direction of travel as follows [78, 86, 127]:

$$P_s = calcium\ event\ probability\ in\ each\ bin$$

$$P_o = occupancy\ probability\ at\ each\ bin$$

$$p = \frac{P_s}{P_o}$$

$$M_s = \sum P_s$$

$$M_o = \sum P_o$$

$$MI = \sum p * \log_2\left(\frac{p}{M_s * M_o}\right)$$

Place field location was determined by the location of maximum firing rate.

Position decoding

Position was decoded using all recorded cells in a session and was decoded for times when the rat was moving (velocity>12cm/s). The track was split in 10cm segments and the time window of decoding was 0.5 seconds with non-overlapping time bins. Decoding was done using Bayesian decoding [81].

$$x = positions, f_i(x) = average\ firing\ rate\ per\ second\ for\ cell\ N\ at\ position\ X$$

$$n = calcium\ events\ per\ cell, n_i = number\ of\ events\ in\ time\ window$$

$$N = total\ number\ of\ cells$$

$$t = time\ window\ of\ decoding$$

$$C(t, n) = normalization\ factor\ for\ probabilities\ to\ equal\ 1$$

$$P(x|n) = odds\ of\ being\ at\ position\ x\ giving\ calcium\ events\ n$$

$$P(x|n) = C(t,n)\left(\prod_{i=1}^{\mathrm{N}} f_i(x)^{n_i}\right)\exp\left(-t\sum_{i=1}^{\mathrm{N}} f_i(x)\right)$$

Accuracy decoding was determined by randomly shuffling firing per position bins and re-decoding. The difference between actual and decoded position was then determined per time bin and compared to decoded shuffled data.

Validation across days and within session

Validation was done using the Matlab-based CIATAH software [76, 77]. Videos underwent 3 rounds of registration comprised of Turboreg image rotation [125]. An image binarization threshold of 40% of the images' maximum value was used to remove background noise and axons and dendrites. A distance threshold of a maximum of 5 pixels was used to match cells across sessions, with a minimum 2-D correlation coefficient of 0.5. All sessions were aligned to the fourth recording session.

.

Figure captions

Figure 1: GCaMP is expressed in the CA1 cell layer of rat hippocampus

a. Diagram showing injection locations of AAV9-Syn-GCaMP7c, right below the CA1 cell layer. There are four total injection sites, with 0.6uL injected at each site. (CC = corpus callosum, DG = dentate gyrus)
b. Diagram showing level of aspiration in brain tissue. The entire corpus callosum is aspirated until the vertical striations of the alveus are visible.
c. GCaMP expression in the hippocampus, taken with a confocal microscope. The CA1 cell layer is labeled.

Figure 2: Hundreds of cells can be captured in a single Ca2+ imaging session

a. Examples of data from two (top and bottom rows) recording sessions. First column: example image from pre-processing. Second column: image post-processing (see materials and methods). Third column: all cell extractions, prior to manual cell sorting. Fourth column: post processing image overlayed with cell outlines identified after manual sorting.
b. Example traces from 15 cells taken during 124 seconds of calcium imaging.
c. Number of cells imaged per session for each rat. Dotted red line indicates the average for each animal.
d. Events/second for cells. Dotted red line indicates the average (0.090+-0.019 events/s)
e. Events/second for individual rats (averages: 0.084+-0.024, 0.074+-0.026, 0.085+-0.020, and 0.116+-0.032 events/second)
f. Average events per second in a session is positively correlated with the animal's average speed in that session
g. There is a positive correlation between events/s and the animal's speed.

Figure 3: Calcium events are correlated with periods of movement

688 a. Raster plot of cell firing during linear track running. Top: the animal's speed.
689 Bottom: raster of peak calcium transients of 352 identified cells.
690 b. Graph showing an example of speed (plotted in black) overlayed with event rate
691 (in blue). Bottom panel is a zoom in of a smaller time period.
692 c. An example logarithmic correlation of animal speed against calcium events/
693 second.
694
695 **Figure 4:** A high percentage of place cells are recorded on the linear track using Ca2+
696 imaging
697 a. Graph showing the percentage of place cells per session for each rat (blue).
698 Analysis was repeated including only cells with a firing rate >0.01Hz during
699 movement (red). Dotted lines indicate the average for each animal.
700 b. Nine example place cells. A firing rate map in both directions of travel is
701 provided for each cell, with the top map corresponding with running to the
702 right, and the bottom map corresponding with running to the left. Note the
703 colorbar scales may be different for each direction of travel. The difference in
704 mutual information scores between the cell and the top 95% of shuffled data
705 (actual MI-shuffled MI) is indicated in the left corner. If the actual MI was
706 greater than 95% of shuffled data, the number is printed in bold white.
707 c. Distribution of directional mutual information scores after shuffling cells seen
708 in figure 3b. Event data was shuffled 500 times and the top 95% of mutual
709 information scores were determined from shuffled data (red dotted line). If the
710 actual mutual information score (green line) was greater than the upper 95%
711 MI score of shuffled data, the cell was considered to be a place cell.
712 d. Top left: Place field maximum event rate during movement (dotted red line
713 indicates average of 0.15events/s). Top right: average firing rate during
714 movement (red line is average at 0.02events/s). Bottom: Increase from
715 average to maximum rate (max/mean). On average, cells increased firing
716 7.4x from their average firing rate during movement to their maximum firing
717 rate (dotted red line indicates average)

Figure 5: Place cells are sufficient to decode the animal's position

a. Four decoding examples as the animal traverses the track. Black line indicates the animal's actual position, with the stars indicated sample point. The colored circles connected by the red line indicate decoded position. The color of the circles indicates decoding certainty.
b. Same as A but decoding is using shuffled units. Decoding is much less accurate using shuffled data.

Figure 6: Individual cells and their place fields can be maintained across sessions

a. Cells can be maintained across sessions weeks apart. Examples from two animals of data taken on the first and final days of recording. Cells are color-matched from the first to last day. Cells in gray represent cells with no matches between the two days. Of note, these recordings were prioritized for cell number as proof of concept rather than maintaining the same landmarks (such as blood vessels) across days.
b. Percent of cells that appeared in different numbers of sessions. Symbols represent averages for individual animals.
c. Percent of cells that had place fields in different numbers of sessions. Symbols represent averages for individual animals.
d. The recurrence probability of a cell based on the number of days between recordings. Recordings from rat 3 were from found to be from two different focal planes.
e. Average recurrence probability across days, excluding rat 3. For every day passing, a cell has a 0.43% less chance of reoccurring.
f. Change in place field location between recording sessions. Included all sessions recorded for an animal; sessions did not need to be adjacent.
g. Place field locations are highly correlated across sessions. We compared place field locations between all sessions of an animal and found field locations to be consistently highly correlated.

h. There was no correlation ($p>0.05$) between r2 value of place field correlations and days elapsed between sessions.

Figure S1: Animals ran on a linear track.

a. Diagram of linear track. The animal would run back and forth between the two sides to receive a pellet reward
b. Trace of animal position over one session

Figure S2: Percentage of cells that would be place cells if the mutual information value exceeded the mean plus three standard deviations of a shuffled distribution. Using this criterion (blue bars), we found that 64.3+-5.1 percent of all cells were place cells, with individual animals at 59.5+-12.0%, 65.5+-2.3%, 61.2+-14%, and 71.0+-12.1%. If we applied the 0.01hz threshold to include cells (red bars), 73.4+-4.3% of cells were place cells, with individual animals at 68.0+-11.8%, 77.6+-5.6%, 77.0+-14.6% and 76.0+-13.0%. Dotted lines indicate averages.

Acknowledgements

We would like to thank all members of the Disterhoft lab, especially Matthew Oh, Craig Weiss, and Kent Park. We would also like to thank the Miniscope team, in particular Daniel Aharoni and Federico Sangiuliano Jimka. We additionally thank Biafra Ahanonu for assistance with CIATAH, Amy Christensen for providing advice during imaging setup, David Wirtshafter for discussion and editing help, and Drew Ames for consultation on figures.

Funding Disclosure

This work was supported by an NIA T32 (T32-AG020506/AG/NIA), an NIA R37 (R37-AG008796/AG/NIA) and an NINDS R01 (R01 NS113804/NS/NINDS).

Competing Interests

The authors declare no competing interests.

Related Manuscripts

Authors do not have a related or duplicate manuscript under consideration (or accepted) for publication elsewhere.

Citations

1. Grienberger C, Konnerth A. Imaging calcium in neurons. Neuron. 2012;73(5):862-85. doi: 10.1016/j.neuron.2012.02.011. PubMed PMID: 22405199.
2. Aharoni D, Hoogland TM. Circuit Investigations With Open-Source Miniaturized Microscopes: Past, Present and Future. Frontiers in cellular neuroscience. 2019;13:141. doi: 10.3389/fncel.2019.00141. PubMed PMID: 31024265; PubMed Central PMCID: PMCPMC6461004.
3. Aharoni D, Khakh BS, Silva AJ, Golshani P. All the light that we can see: a new era in miniaturized microscopy. Nat Methods. 2019;16(1):11-3. doi: 10.1038/s41592-018-0266-x. PubMed PMID: 30573833.
4. Rickgauer JP, Deisseroth K, Tank DW. Simultaneous cellular-resolution optical perturbation and imaging of place cell firing fields. Nat Neurosci. 2014;17(12):1816-24. doi: 10.1038/nn.3866. PubMed PMID: 25402854; PubMed Central PMCID: PMCPMC4459599.
5. Resendez SL, Jennings JH, Ung RL, Namboodiri VM, Zhou ZC, Otis JM, et al. Visualization of cortical, subcortical and deep brain neural circuit dynamics during naturalistic mammalian behavior with head-mounted microscopes and chronically implanted lenses. Nature protocols. 2016;11(3):566-97. Epub 2016/02/26. doi: 10.1038/nprot.2016.021. PubMed PMID: 26914316; PubMed Central PMCID: PMCPMC5239057.
6. Grienberger C, Konnerth A. Imaging calcium in neurons. Neuron. 2012;73(5):862-85.
7. Hamel EJ, Grewe BF, Parker JG, Schnitzer MJ. Cellular level brain imaging in behaving mammals: an engineering approach. Neuron. 2015;86(1):140-59. Epub 2015/04/10. doi: 10.1016/j.neuron.2015.03.055. PubMed PMID: 25856491; PubMed Central PMCID: PMCPMC5758309.
8. Zhou H, Neville KR, Goldstein N, Kabu S, Kausar N, Ye R, et al. Cholinergic modulation of hippocampal calcium activity across the sleep-wake cycle. eLife. 2019;8. Epub 2019/03/08. doi: 10.7554/eLife.39777. PubMed PMID: 30843520; PubMed Central PMCID: PMCPMC6435325.
9. Sheintuch L, Rubin A, Brande-Eilat N, Geva N, Sadeh N, Pinchasof O, et al. Tracking the Same Neurons across Multiple Days in Ca(2+) Imaging Data. Cell reports. 2017;21(4):1102-15. doi: 10.1016/j.celrep.2017.10.013. PubMed PMID: 29069591; PubMed Central PMCID: PMCPMC5670033.
10. Hainmueller T, Bartos M. Parallel emergence of stable and dynamic memory engrams in the hippocampus. Nature. 2018;558(7709):292-6. doi: 10.1038/s41586-018-0191-2. PubMed PMID: 29875406.
11. Dombeck DA, Harvey CD, Tian L, Looger LL, Tank DW. Functional imaging of hippocampal place cells at cellular resolution during virtual navigation. Nat Neurosci. 2010;13(11):1433-40. doi: 10.1038/nn.2648. PubMed PMID: 20890294; PubMed Central PMCID: PMCPMC2967725.
12. Kinsky NR, Mau W, Sullivan DW, Levy SJ, Ruesch EA, Hasselmo ME. Trajectory-modulated hippocampal neurons persist throughout memory-guided navigation. Nature communications. 2020;11(1):2443. Epub 2020/05/18. doi: 10.1038/s41467-020-16226-4. PubMed PMID: 32415083; PubMed Central PMCID: PMCPMC7229120.

13. Sheintuch L, Geva N, Baumer H, Rechavi Y, Rubin A, Ziv Y. Multiple Maps of the Same Spatial Context Can Stably Coexist in the Mouse Hippocampus. Current biology : CB. 2020;30(8):1467-76 e6. Epub 2020/03/30. doi: 10.1016/j.cub.2020.02.018. PubMed PMID: 32220328.

14. Ziv Y, Burns LD, Cocker ED, Hamel EO, Ghosh KK, Kitch LJ, et al. Long-term dynamics of CA1 hippocampal place codes. Nat Neurosci. 2013;16(3):264-6. Epub 2013/02/12. doi: 10.1038/nn.3329. PubMed PMID: 23396101; PubMed Central PMCID: PMCPMC3784308.

15. Cai DJ, Aharoni D, Shuman T, Shobe J, Biane J, Song W, et al. A shared neural ensemble links distinct contextual memories encoded close in time. Nature. 2016;534(7605):115-8. Epub 2016/06/03. doi: 10.1038/nature17955. PubMed PMID: 27251287; PubMed Central PMCID: PMCPMC5063500.

16. Jimenez JC, Berry JE, Lim SC, Ong SK, Kheirbek MA, Hen R. Contextual fear memory retrieval by correlated ensembles of ventral CA1 neurons. Nature communications. 2020;11(1):3492. Epub 2020/07/15. doi: 10.1038/s41467-020-17270-w. PubMed PMID: 32661319; PubMed Central PMCID: PMCPMC7359370.

17. Zhang X, Li B. Population coding of valence in the basolateral amygdala. Nature communications. 2018;9(1):5195. Epub 2018/12/07. doi: 10.1038/s41467-018-07679-9. PubMed PMID: 30518754; PubMed Central PMCID: PMCPMC6281657.

18. Shuman T, Aharoni D, Cai DJ, Lee CR, Chavlis S, Page-Harley L, et al. Breakdown of spatial coding and interneuron synchronization in epileptic mice. Nat Neurosci. 2020;23(2):229-38. Epub 2020/01/08. doi: 10.1038/s41593-019-0559-0. PubMed PMID: 31907437; PubMed Central PMCID: PMCPMC7259114.

19. Shin JH, Song M, Paik SB, Jung MW. Spatial organization of functional clusters representing reward and movement information in the striatal direct and indirect pathways. Proc Natl Acad Sci U S A. 2020;117(43):27004-15. Epub 2020/10/16. doi: 10.1073/pnas.2010361117. PubMed PMID: 33055217; PubMed Central PMCID: PMCPMC7604453.

20. Wang X, Liu Y, Li X, Zhang Z, Yang H, Zhang Y, et al. Deconstruction of Corticospinal Circuits for Goal-Directed Motor Skills. Cell. 2017;171(2):440-55 e14. Epub 2017/09/26. doi: 10.1016/j.cell.2017.08.014. PubMed PMID: 28942925; PubMed Central PMCID: PMCPMC5679421.

21. Klaus A, Martins GJ, Paixao VB, Zhou P, Paninski L, Costa RM. The Spatiotemporal Organization of the Striatum Encodes Action Space. Neuron. 2017;95(5):1171-80 e7. Epub 2017/09/01. doi: 10.1016/j.neuron.2017.08.015. PubMed PMID: 28858619; PubMed Central PMCID: PMCPMC5584673.

22. Guo W, Zhang JJ, Newman JP, Wilson MA. Latent learning drives sleep-dependent plasticity in distinct CA1 subpopulations. bioRxiv. 2020:2020.02.27.967794. doi: 10.1101/2020.02.27.967794.

23. O'Keefe J. Place units in the hippocampus of the freely moving rat. Exp Neurol. 1976;51(1):78-109. Epub 1976/04/01. PubMed PMID: 1261644.

24. Wilson MA, McNaughton BL. Dynamics of the hippocampal ensemble code for space. Science. 1993;261(5124):1055-8. Epub 1993/08/20. PubMed PMID: 8351520.

25. Leutgeb S, Leutgeb JK, Treves A, Moser MB, Moser EI. Distinct ensemble codes in hippocampal areas CA3 and CA1. Science. 2004;305(5688):1295-8. Epub 2004/07/24. doi: 10.1126/science.1100265
1100265 [pii]. PubMed PMID: 15272123.
26. McEchron MD, Disterhoft JF. Hippocampal encoding of non-spatial trace conditioning. Hippocampus. 1999;9(4):385-96. doi: 10.1002/(SICI)1098-1063(1999)9:4<385::AID-HIPO5>3.0.CO;2-K. PubMed PMID: 10495020.
27. Schimanski LA, Lipa P, Barnes CA. Tracking the course of hippocampal representations during learning: when is the map required? J Neurosci. 2013;33(7):3094-106. doi: 10.1523/JNEUROSCI.1348-12.2013. PubMed PMID: 23407964; PubMed Central PMCID: PMCPMC3700421.
28. Stefanini F, Kushnir L, Jimenez JC, Jennings JH, Woods NI, Stuber GD, et al. A Distributed Neural Code in the Dentate Gyrus and in CA1. Neuron. 2020;107(4):703-16 e4. Epub 2020/06/11. doi: 10.1016/j.neuron.2020.05.022. PubMed PMID: 32521223; PubMed Central PMCID: PMCPMC7442694.
29. Scoville WB, Milner B. Loss of recent memory after bilateral hippocampal lesions. Journal of neurology, neurosurgery, and psychiatry. 1957;20(1):11-21. Epub 1957/02/01. PubMed PMID: 13406589; PubMed Central PMCID: PMC497229.
30. Squire LR. Memory and the hippocampus: a synthesis from findings with rats, monkeys, and humans. Psychol Rev. 1992;99(2):195-231. Epub 1992/04/01. PubMed PMID: 1594723.
31. Hasselmo ME, McClelland JL. Neural models of memory. Curr Opin Neurobiol. 1999;9(2):184-8. Epub 1999/05/14. doi: S0959-4388(99)80025-7 [pii]. PubMed PMID: 10322183.
32. Ferbinteanu J, Shapiro ML. Prospective and retrospective memory coding in the hippocampus. Neuron. 2003;40(6):1227-39. Epub 2003/12/23. doi: S0896627303007529 [pii]. PubMed PMID: 14687555.
33. Smith DM, Mizumori SJ. Hippocampal place cells, context, and episodic memory. Hippocampus. 2006;16(9):716-29. Epub 2006/08/10. doi: 10.1002/hipo.20208. PubMed PMID: 16897724.
34. Vann SD. Dismantling the Papez circuit for memory in rats. eLife. 2013;2:e00736. Epub 2013/06/28. doi: 10.7554/eLife.00736. PubMed PMID: 23805381; PubMed Central PMCID: PMC3691571.
35. Josselyn SA, Tonegawa S. Memory engrams: Recalling the past and imagining the future. Science. 2020;367(6473). Epub 2020/01/04. doi: 10.1126/science.aaw4325. PubMed PMID: 31896692.
36. Eichenbaum H, Dudchenko P, Wood E, Shapiro M, Tanila H. The hippocampus, memory, and place cells: is it spatial memory or a memory space? Neuron. 1999;23(2):209-26. Epub 1999/07/10. doi: S0896-6273(00)80773-4 [pii]. PubMed PMID: 10399928.
37. Ferbinteanu J, Kennedy PJ, Shapiro ML. Episodic memory—from brain to mind. Hippocampus. 2006;16(9):691-703.
38. McNaughton BL, Battaglia FP, Jensen O, Moser EI, Moser MB. Path integration and the neural basis of the 'cognitive map'. Nat Rev Neurosci. 2006;7(8):663-78. Epub 2006/07/22. doi: nrn1932 [pii]
10.1038/nrn1932. PubMed PMID: 16858394.

39. Foster DJ, Knierim JJ. Sequence learning and the role of the hippocampus in rodent navigation. Curr Opin Neurobiol. 2012;22(2):294-300. Epub 2012/01/10. doi: 10.1016/j.conb.2011.12.005
S0959-4388(11)00223-6 [pii]. PubMed PMID: 22226994.
40. Foster DJ, Morris RG, Dayan P. A model of hippocampally dependent navigation, using the temporal difference learning rule. Hippocampus. 2000;10(1):1-16. Epub 2000/03/08. doi: 10.1002/(SICI)1098-1063(2000)10:1<1::AID-HIPO1>3.0.CO;2-1. PubMed PMID: 10706212.
41. Avigan PD, Cammack K, Shapiro ML. Flexible spatial learning requires both the dorsal and ventral hippocampus and their functional interactions with the prefrontal cortex. Hippocampus. 2020;30(7):733-44.
42. Moser EI, Moser M-B, McNaughton BL. Spatial representation in the hippocampal formation: a history. Nature neuroscience. 2017;20(11):1448-64.
43. Rosenzweig ES, Redish AD, McNaughton BL, Barnes CA. Hippocampal map realignment and spatial learning. Nature neuroscience. 2003;6(6):609-15.
44. Moyer JR, Jr., Deyo RA, Disterhoft JF. Hippocampectomy disrupts trace eye-blink conditioning in rabbits. Behav Neurosci. 1990;104(2):243-52. PubMed PMID: 2346619.
45. Andrzejewski ME, Ryals C. Dissociable hippocampal and amygdalar D1-like receptor contribution to discriminated Pavlovian conditioned approach learning. Behav Brain Res. 2016;299:111-21. doi: 10.1016/j.bbr.2015.11.034. PubMed PMID: 26632336; PubMed Central PMCID: PMCPMC4866504.
46. Ito R, Everitt BJ, Robbins TW. The hippocampus and appetitive Pavlovian conditioning: effects of excitotoxic hippocampal lesions on conditioned locomotor activity and autoshaping. Hippocampus. 2005;15(6):713-21. doi: 10.1002/hipo.20094. PubMed PMID: 15906393.
47. Chan KH, Morell JR, Jarrard LE, Davidson TL. Reconsideration of the role of the hippocampus in learned inhibition. Behav Brain Res. 2001;119(2):111-30. PubMed PMID: 11165328.
48. Pritchard A, Hornung R, Kramer PR. Measuring calcium activity within individual neurons within the rat thalamus. MethodsX. 2021;8:101273.
49. Anner P, Passecker J, Klausberger T, Dorffner G. Ca2+ imaging of neurons in freely moving rats with automatic post hoc histological identification. Journal of neuroscience methods. 2020;341:108765.
50. Scott BB, Thiberge SY, Guo C, Tervo DGR, Brody CD, Karpova AY, et al. Imaging cortical dynamics in GCaMP transgenic rats with a head-mounted widefield macroscope. Neuron. 2018;100(5):1045-58. e5.
51. Hart EE, Blair GJ, O'Dell TJ, Blair HT, Izquierdo A. Chemogenetic modulation and single-photon calcium imaging in anterior cingulate cortex reveal a mechanism for effort-based decisions. Journal of Neuroscience. 2020;40(29):5628-43.
52. Swanson L. Brain maps: structure of the rat brain: Gulf Professional Publishing; 2004.
53. Franklin KBJ, Paxinos G. Paxinos and Franklin's The mouse brain in stereotaxic coordinates2013.
54. Routh BN, Johnston D, Harris K, Chitwood RA. Anatomical and electrophysiological comparison of CA1 pyramidal neurons of the rat and mouse. Journal of neurophysiology. 2009;102(4):2288-302.

960 55. Whishaw IQ. A comparison of rats and mice in a swimming pool place task and matching
961 to place task: some surprising differences. Physiol Behav. 1995;58(4):687-93. Epub 1995/10/01.
962 doi: 10.1016/0031-9384(95)00110-5. PubMed PMID: 8559777.
963 56. Frick KM, Stillner ET, Berger-Sweeney J. Mice are not little rats: species differences in a
964 one-day water maze task. Neuroreport. 2000;11(16):3461-5. Epub 2000/11/30. doi:
965 10.1097/00001756-200011090-00013. PubMed PMID: 11095500.
966 57. Rosenfeld CS, Ferguson SA. Barnes maze testing strategies with small and large rodent
967 models. J Vis Exp. 2014;(84):e51194. Epub 2014/03/19. doi: 10.3791/51194. PubMed PMID:
968 24637673; PubMed Central PMCID: PMCPMC4140524.
969 58. Cressant A, Besson M, Suarez S, Cormier A, Granon S. Spatial learning in Long-Evans
970 Hooded rats and C57BL/6J mice: different strategies for different performance. Behav Brain
971 Res. 2007;177(1):22-9. Epub 2006/12/13. doi: 10.1016/j.bbr.2006.11.010. PubMed PMID:
972 17157932.
973 59. Hok V, Poucet B, Duvelle É, Save É, Sargolini F. Spatial cognition in mice and rats:
974 similarities and differences in brain and behavior. Wiley Interdisciplinary Reviews: Cognitive
975 Science. 2016;7(6):406-21.
976 60. Whishaw IQ, Metz GA, Kolb B, Pellis SM. Accelerated nervous system development
977 contributes to behavioral efficiency in the laboratory mouse: a behavioral review and
978 theoretical proposal. Developmental Psychobiology: The Journal of the International Society for
979 Developmental Psychobiology. 2001;39(3):151-70.
980 61. Vengeliene V, Bilbao A, Spanagel R. The alcohol deprivation effect model for studying
981 relapse behavior: a comparison between rats and mice. Alcohol. 2014;48(3):313-20. Epub
982 2014/05/09. doi: 10.1016/j.alcohol.2014.03.002. PubMed PMID: 24811155.
983 62. Carter CS, Richardson A, Huffman DM, Austad S. Bring Back the Rat! J Gerontol A Biol Sci
984 Med Sci. 2020;75(3):405-15. Epub 2020/01/03. doi: 10.1093/gerona/glz298. PubMed PMID:
985 31894235; PubMed Central PMCID: PMCPMC7021637.
986 63. Ellenbroek B, Youn J. Rodent models in neuroscience research: is it a rat race? Dis Model
987 Mech. 2016;9(10):1079-87. Epub 2016/10/14. doi: 10.1242/dmm.026120. PubMed PMID:
988 27736744; PubMed Central PMCID: PMCPMC5087838.
989 64. Iannaccone PM, Jacob HJ. Rats! Dis Model Mech. 2009;2(5-6):206-10. Epub 2009/05/02.
990 doi: 10.1242/dmm.002733. PubMed PMID: 19407324; PubMed Central PMCID:
991 PMCPMC2675817.
992 65. Buerge T, Weiss T. Handling and Restraint. In: Hedrich HJ, Bullock G, editors. The
993 Laboratory Mouse (Handbook of Experimental Animals): Elsevier; 2004. p. 517-26.
994 66. Voigts J, Newman JP, Wilson MA, Harnett MT. An easy-to-assemble, robust, and
995 lightweight drive implant for chronic tetrode recordings in freely moving animals. J Neural Eng.
996 2020;17(2):026044. Epub 2020/02/20. doi: 10.1088/1741-2552/ab77f9. PubMed PMID:
997 32074511.
998 67. Voigts J, Siegle JH, Pritchett DL, Moore CI. The flexDrive: an ultra-light implant for optical
999 control and highly parallel chronic recording of neuronal ensembles in freely moving mice.
1000 Front Syst Neurosci. 2013;7:8. Epub 2013/05/30. doi: 10.3389/fnsys.2013.00008. PubMed
1001 PMID: 23717267; PubMed Central PMCID: PMCPMC3652307.

1002 68. Bolkvadze T, Pitkanen A. Development of post-traumatic epilepsy after controlled
1003 cortical impact and lateral fluid-percussion-induced brain injury in the mouse. J Neurotrauma.
1004 2012;29(5):789-812. Epub 2011/10/26. doi: 10.1089/neu.2011.1954. PubMed PMID: 22023672.
1005 69. Hunt RF, Scheff SW, Smith BN. Posttraumatic epilepsy after controlled cortical impact
1006 injury in mice. Exp Neurol. 2009;215(2):243-52. Epub 2008/11/18. doi:
1007 10.1016/j.expneurol.2008.10.005. PubMed PMID: 19013458; PubMed Central PMCID:
1008 PMCPMC4694635.
1009 70. Hunt RF, Scheff SW, Smith BN. Regionally localized recurrent excitation in the dentate
1010 gyrus of a cortical contusion model of posttraumatic epilepsy. J Neurophysiol.
1011 2010;103(3):1490-500. Epub 2010/01/22. doi: 10.1152/jn.00957.2009. PubMed PMID:
1012 20089815; PubMed Central PMCID: PMCPMC2887624.
1013 71. Steinmetz NA, Buetfering C, Lecoq J, Lee CR, Peters AJ, Jacobs EAK, et al. Aberrant
1014 Cortical Activity in Multiple GCaMP6-Expressing Transgenic Mouse Lines. eNeuro. 2017;4(5).
1015 Epub 2017/09/22. doi: 10.1523/ENEURO.0207-17.2017. PubMed PMID: 28932809; PubMed
1016 Central PMCID: PMCPMC5604087.
1017 72. Yang Y, Liu N, He Y, Liu Y, Ge L, Zou L, et al. Improved calcium sensor GCaMP-X
1018 overcomes the calcium channel perturbations induced by the calmodulin in GCaMP. Nature
1019 communications. 2018;9(1):1504. Epub 2018/04/19. doi: 10.1038/s41467-018-03719-6.
1020 PubMed PMID: 29666364; PubMed Central PMCID: PMCPMC5904127.
1021 73. Tian L, Hires SA, Mao T, Huber D, Chiappe ME, Chalasani SH, et al. Imaging neural
1022 activity in worms, flies and mice with improved GCaMP calcium indicators. Nat Methods.
1023 2009;6(12):875-81. Epub 2009/11/10. doi: 10.1038/nmeth.1398. PubMed PMID: 19898485;
1024 PubMed Central PMCID: PMCPMC2858873.
1025 74. Nathanson JL, Yanagawa Y, Obata K, Callaway EM. Preferential labeling of inhibitory and
1026 excitatory cortical neurons by endogenous tropism of adeno-associated virus and lentivirus
1027 vectors. Neuroscience. 2009;161(2):441-50. Epub 2009/03/26. doi:
1028 10.1016/j.neuroscience.2009.03.032. PubMed PMID: 19318117; PubMed Central PMCID:
1029 PMCPMC2728494.
1030 75. Zhou P, Resendez SL, Rodriguez-Romaguera J, Jimenez JC, Neufeld SQ, Giovannucci A, et
1031 al. Efficient and accurate extraction of in vivo calcium signals from microendoscopic video data.
1032 eLife. 2018;7. Epub 2018/02/23. doi: 10.7554/eLife.28728. PubMed PMID: 29469809; PubMed
1033 Central PMCID: PMCPMC5871355.
1034 76. Ahanonu B. CIAtah: a software package for analyzing one- and two-photon calcium
1035 imaging datasets. v1.0.0 ed: Zenodo; 2018.
1036 77. Corder G, Ahanonu B, Grewe BF, Wang D, Schnitzer MJ, Scherrer G. An amygdalar neural
1037 ensemble that encodes the unpleasantness of pain. Science. 2019;363(6424):276-81. Epub
1038 2019/01/19. doi: 10.1126/science.aap8586. PubMed PMID: 30655440; PubMed Central PMCID:
1039 PMCPMC6450685.
1040 78. Kinsky NR, Sullivan DW, Mau W, Hasselmo ME, Eichenbaum HB. Hippocampal Place
1041 Fields Maintain a Coherent and Flexible Map across Long Timescales. Current biology : CB.
1042 2018;28(22):3578-88 e6. Epub 2018/11/06. doi: 10.1016/j.cub.2018.09.037. PubMed PMID:
1043 30393037; PubMed Central PMCID: PMCPMC6331214.

79. Wilent WB, Nitz DA. Discrete place fields of hippocampal formation interneurons. J Neurophysiol. 2007;97(6):4152-61. Epub 2007/03/30. doi: 10.1152/jn.01200.2006. PubMed PMID: 17392415.
80. Ego-Stengel V, Wilson MA. Spatial selectivity and theta phase precession in CA1 interneurons. Hippocampus. 2007;17(2):161-74. doi: 10.1002/hipo.20253. PubMed PMID: 17183531.
81. Zhang K, Ginzburg I, McNaughton BL, Sejnowski TJ. Interpreting neuronal population activity by reconstruction: unified framework with application to hippocampal place cells. J Neurophysiol. 1998;79(2):1017-44. doi: 10.1152/jn.1998.79.2.1017. PubMed PMID: 9463459.
82. Meshulam L, Gauthier JL, Brody CD, Tank DW, Bialek W. Collective Behavior of Place and Non-place Neurons in the Hippocampal Network. Neuron. 2017;96(5):1178-91 e4. Epub 2017/11/21. doi: 10.1016/j.neuron.2017.10.027. PubMed PMID: 29154129; PubMed Central PMCID: PMCPMC5720931.
83. Jun H, Bramian A, Soma S, Saito T, Saido TC, Igarashi KM. Disrupted Place Cell Remapping and Impaired Grid Cells in a Knockin Model of Alzheimer's Disease. Neuron. 2020;107(6):1095-112 e6. Epub 2020/07/23. doi: 10.1016/j.neuron.2020.06.023. PubMed PMID: 32697942; PubMed Central PMCID: PMCPMC7529950.
84. Rich PD, Liaw HP, Lee AK. Place cells. Large environments reveal the statistical structure governing hippocampal representations. Science. 2014;345(6198):814-7. doi: 10.1126/science.1255635. PubMed PMID: 25124440.
85. Souza BC, Pavão R, Belchior H, Tort AB. On information metrics for spatial coding. Neuroscience. 2018;375:62-73.
86. Wirtshafter HS, Wilson MA. Differences in reward biased spatial representations in the lateral septum and hippocampus. eLife. 2020;9. Epub 2020/05/27. doi: 10.7554/eLife.55252. PubMed Central PMCID: PMCPMC7274787.
87. Stefanini F, Kushnir L, Jimenez JC, Jennings JH, Woods NI, Stuber GD, et al. A distributed neural code in the dentate gyrus and in CA1. Neuron. 2020;107(4):703-16. e4.
88. Mou X, Cheng J, Yu YS, Kee SE, Ji D. Comparing mouse and rat hippocampal place cell activities and firing sequences in the same environments. Frontiers in cellular neuroscience. 2018;12:332.
89. Huang L, Ledochowitsch P, Knoblich U, Lecoq J, Murphy GJ, Reid RC, et al. Relationship between simultaneously recorded spiking activity and fluorescence signal in GCaMP6 transgenic mice. eLife. 2021;10:e51675.
90. Fenton AA, Kao H-Y, Neymotin SA, Olypher A, Vayntrub Y, Lytton WW, et al. Unmasking the CA1 ensemble place code by exposures to small and large environments: more place cells and multiple, irregularly arranged, and expanded place fields in the larger space. Journal of Neuroscience. 2008;28(44):11250-62.
91. Markus EJ, Barnes CA, McNaughton BL, Gladden VL, Skaggs WE. Spatial information content and reliability of hippocampal CA1 neurons: effects of visual input. Hippocampus. 1994;4(4):410-21.
92. Podor B, Hu YL, Ohkura M, Nakai J, Croll R, Fine A. Comparison of genetically encoded calcium indicators for monitoring action potentials in mammalian brain by two-photon excitation fluorescence microscopy. Neurophotonics. 2015;2(2):021014. Epub 2015/07/15. doi:

10.1117/1.NPh.2.2.021014. PubMed PMID: 26158004; PubMed Central PMCID: PMCPMC4478877.
93. Chen TW, Wardill TJ, Sun Y, Pulver SR, Renninger SL, Baohan A, et al. Ultrasensitive fluorescent proteins for imaging neuronal activity. Nature. 2013;499(7458):295-300. Epub 2013/07/23. doi: 10.1038/nature12354. PubMed PMID: 23868258.
94. Shemesh OA, Linghu C, Piatkevich KD, Goodwin D, Celiker OT, Gritton HJ, et al. Precision Calcium Imaging of Dense Neural Populations via a Cell-Body-Targeted Calcium Indicator. Neuron. 2020;107(3):470-86 e11. Epub 2020/06/28. doi: 10.1016/j.neuron.2020.05.029. PubMed PMID: 32592656; PubMed Central PMCID: PMCPMC7415598.
95. Tian L, Hires SA, Mao T, Huber D, Chiappe ME, Chalasani SH, et al. Imaging neural activity in worms, flies and mice with improved GCaMP calcium indicators. Nature methods. 2009;6(12):875-81.
96. Podor B, Hu Y-l, Ohkura M, Nakai J, Croll R, Fine A. Comparison of genetically encoded calcium indicators for monitoring action potentials in mammalian brain by two-photon excitation fluorescence microscopy. Neurophotonics. 2015;2(2):021014.
97. Guzowski JF, McNaughton BL, Barnes CA, Worley PF. Environment-specific expression of the immediate-early gene Arc in hippocampal neuronal ensembles. Nat Neurosci. 1999;2(12):1120-4. Epub 1999/11/26. doi: 10.1038/16046. PubMed PMID: 10570490.
98. Witharana WK, Cardiff J, Chawla MK, Xie JY, Alme CB, Eckert M, et al. Nonuniform allocation of hippocampal neurons to place fields across all hippocampal subfields. Hippocampus. 2016;26(10):1328-44. Epub 2016/06/09. doi: 10.1002/hipo.22609. PubMed PMID: 27273259.
99. McNaughton BL, Barnes CA, O'Keefe J. The contributions of position, direction, and velocity to single unit activity in the hippocampus of freely-moving rats. Experimental brain research. 1983;52(1):41-9.
100. Chrobak JJ, Buzsaki G. High-frequency oscillations in the output networks of the hippocampal-entorhinal axis of the freely behaving rat. J Neurosci. 1996;16(9):3056-66. Epub 1996/05/01. PubMed PMID: 8622135.
101. Csicsvari J, Hirase H, Czurko A, Mamiya A, Buzsaki G. Fast network oscillations in the hippocampal CA1 region of the behaving rat. J Neurosci. 1999;19(16):RC20. Epub 1999/08/06. PubMed PMID: 10436076.
102. Kudrimoti HS, Barnes CA, McNaughton BL. Reactivation of hippocampal cell assemblies: effects of behavioral state, experience, and EEG dynamics. J Neurosci. 1999;19(10):4090-101. Epub 1999/05/11. PubMed PMID: 10234037; PubMed Central PMCID: PMCPMC6782694.
103. Ylinen A, Bragin A, Nadasdy Z, Jando G, Szabo I, Sik A, et al. Sharp wave-associated high-frequency oscillation (200 Hz) in the intact hippocampus: network and intracellular mechanisms. J Neurosci. 1995;15(1 Pt 1):30-46. Epub 1995/01/01. PubMed PMID: 7823136.
104. Buzsaki G. Two-stage model of memory trace formation: a role for "noisy" brain states. Neuroscience. 1989;31(3):551-70. Epub 1989/01/01. doi: 0306-4522(89)90423-5 [pii]. PubMed PMID: 2687720.
105. Colgin LL. Mechanisms and functions of theta rhythms. Annu Rev Neurosci. 2013;36:295-312. doi: 10.1146/annurev-neuro-062012-170330. PubMed PMID: 23724998.

1129 106. Hasselmo ME. What is the function of hippocampal theta rhythm?--Linking behavioral
1130 data to phasic properties of field potential and unit recording data. Hippocampus.
1131 2005;15(7):936-49. doi: 10.1002/hipo.20116. PubMed PMID: 16158423.
1132 107. Hasselmo ME, Hay J, Ilyn M, Gorchetchnikov A. Neuromodulation, theta rhythm and rat
1133 spatial navigation. Neural Netw. 2002;15(4-6):689-707. Epub 2002/10/10. doi: S0893-
1134 6080(02)00057-6 [pii]. PubMed PMID: 12371520.
1135 108. Wikenheiser AM, Redish AD. Hippocampal theta sequences reflect current goals. Nat
1136 Neurosci. 2015;18(2):289-94. Epub 2015/01/07. doi: 10.1038/nn.3909. PubMed PMID:
1137 25559082; PubMed Central PMCID: PMC4428659.
1138 109. Wirtshafter HS, Wilson MA. Lateral septum as a nexus for mood, motivation, and
1139 movement. Neurosci Biobehav Rev. 2021;126:544-59. Epub 2021/04/14. doi:
1140 10.1016/j.neubiorev.2021.03.029. PubMed PMID: 33848512.
1141 110. Shirvalkar PR, Rapp PR, Shapiro ML. Bidirectional changes to hippocampal theta–gamma
1142 comodulation predict memory for recent spatial episodes. Proceedings of the National
1143 Academy of Sciences. 2010;107(15):7054-9.
1144 111. Colgin LL, Kubota D, Jia Y, Rex CS, Lynch G. Long-term potentiation is impaired in rat
1145 hippocampal slices that produce spontaneous sharp waves. J Physiol. 2004;558(Pt 3):953-61.
1146 Epub 2004/06/15. doi: 10.1113/jphysiol.2004.068080. PubMed PMID: 15194734; PubMed
1147 Central PMCID: PMCPMC1665012.
1148 112. Maier N, Nimmrich V, Draguhn A. Cellular and network mechanisms underlying
1149 spontaneous sharp wave-ripple complexes in mouse hippocampal slices. J Physiol. 2003;550(Pt
1150 3):873-87. Epub 2003/06/17. doi: 10.1113/jphysiol.2003.044602. PubMed PMID: 12807984;
1151 PubMed Central PMCID: PMCPMC2343079.
1152 113. Levy SJ, Kinsky NR, Mau W, Sullivan DW, Hasselmo ME. Hippocampal spatial memory
1153 representations in mice are heterogeneously stable. Hippocampus. 2021;31(3):244-60. Epub
1154 2020/10/25. doi: 10.1002/hipo.23272. PubMed PMID: 33098619; PubMed Central PMCID:
1155 PMCPMC7983370.
1156 114. Mau W, Sullivan DW, Kinsky NR, Hasselmo ME, Howard MW, Eichenbaum H. The Same
1157 Hippocampal CA1 Population Simultaneously Codes Temporal Information over Multiple
1158 Timescales. Current biology : CB. 2018;28(10):1499-508 e4. Epub 2018/05/01. doi:
1159 10.1016/j.cub.2018.03.051. PubMed PMID: 29706516; PubMed Central PMCID:
1160 PMCPMC5964012.
1161 115. Hirst WD, Abrahamsen B, Blaney FE, Calver AR, Aloj L, Price GW, et al. Differences in the
1162 central nervous system distribution and pharmacology of the mouse 5-hydroxytryptamine-6
1163 receptor compared with rat and human receptors investigated by radioligand binding, site-
1164 directed mutagenesis, and molecular modeling. Molecular pharmacology. 2003;64(6):1295-308.
1165 116. Snyder JS, Choe JS, Clifford MA, Jeurling SI, Hurley P, Brown A, et al. Adult-born
1166 hippocampal neurons are more numerous, faster maturing, and more involved in behavior in
1167 rats than in mice. Journal of Neuroscience. 2009;29(46):14484-95.
1168 117. Parker CC, Chen H, Flagel SB, Geurts AM, Richards JB, Robinson TE, et al. Rats are the
1169 smart choice: rationale for a renewed focus on rats in behavioral genetics. Neuropharmacology.
1170 2014;76:250-8.
1171 118. Jupp B, Caprioli D, Dalley JW. Highly impulsive rats: modelling an endophenotype to
1172 determine the neurobiological, genetic and environmental mechanisms of addiction. Dis Model

1173 Mech. 2013;6(2):302-11. Epub 2013/01/29. doi: 10.1242/dmm.010934. PubMed PMID:
1174 23355644; PubMed Central PMCID: PMCPMC3597013.
1175 119. Schoenfeld G, Carta S, Rupprecht P, Ayaz A, Helmchen F. In vivo calcium imaging of CA3
1176 pyramidal neuron populations in adult mouse hippocampus. eNeuro. 2021. Epub 2021/08/01.
1177 doi: 10.1523/ENEURO.0023-21.2021. PubMed PMID: 34330817.
1178 120. Chen LJ, Wang YJ, Chen JR, Tseng GF. Hydrocephalus compacted cortex and
1179 hippocampus and altered their output neurons in association with spatial learning and memory
1180 deficits in rats. Brain Pathol. 2017;27(4):419-36. Epub 2016/07/14. doi: 10.1111/bpa.12414.
1181 PubMed PMID: 27411167; PubMed Central PMCID: PMCPMC8029119.
1182 121. Shim I, Ha Y, Chung JY, Lee HJ, Yang KH, Chang JW. Association of learning and memory
1183 impairments with changes in the septohippocampal cholinergic system in rats with kaolin-
1184 induced hydrocephalus. Neurosurgery. 2003;53(2):416-25; discussion 25. Epub 2003/08/20.
1185 doi: 10.1227/01.neu.0000073989.07810.d8. PubMed PMID: 12925261.
1186 122. Aharoni D, Hoogland TM. Circuit investigations with open-source miniaturized
1187 microscopes: past, present and future. Frontiers in cellular neuroscience. 2019;13:141.
1188 123. Silva AJ. Miniaturized two-photon microscope: seeing clearer and deeper into the brain.
1189 Light: Science & Applications. 2017;6(8):e17104-e.
1190 124. Lopes G, Bonacchi N, Frazao J, Neto JP, Atallah BV, Soares S, et al. Bonsai: an event-
1191 based framework for processing and controlling data streams. Front Neuroinform. 2015;9:7.
1192 Epub 2015/04/24. doi: 10.3389/fninf.2015.00007. PubMed PMID: 25904861; PubMed Central
1193 PMCID: PMCPMC4389726.
1194 125. Thevenaz P, Ruttimann UE, Unser M. A pyramid approach to subpixel registration based
1195 on intensity. IEEE Trans Image Process. 1998;7(1):27-41. Epub 2008/02/13. doi:
1196 10.1109/83.650848. PubMed PMID: 18267377.
1197 126. Wirtshafter HS, Wilson MA. Locomotor and Hippocampal Processing Converge in the
1198 Lateral Septum. Current biology : CB. 2019;29(19):3177-92. doi: 10.1016/j.cub.2019.07.089.
1199 PubMed PMID: 31543450.
1200 127. Olypher AV, Lansky P, Muller RU, Fenton AA. Quantifying location-specific information in
1201 the discharge of rat hippocampal place cells. J Neurosci Methods. 2003;127(2):123-35. Epub
1202 2003/08/09. doi: 10.1016/s0165-0270(03)00123-7. PubMed PMID: 12906942.
1203 128. Talbot ZN, Sparks FT, Dvorak D, Curran BM, Alarcon JM, Fenton AA. Normal CA1 Place
1204 Fields but Discoordinated Network Discharge in a Fmr1-Null Mouse Model of Fragile X
1205 Syndrome. Neuron. 2018;97(3):684-97 e4. Epub 2018/01/24. doi:
1206 10.1016/j.neuron.2017.12.043. PubMed PMID: 29358017; PubMed Central PMCID:
1207 PMCPMC6066593.
1208 129. Maurer AP, Cowen SL, Burke SN, Barnes CA, McNaughton BL. Organization of
1209 hippocampal cell assemblies based on theta phase precession. Hippocampus. 2006;16(9):785-
1210 94. Epub 2006/08/22. doi: 10.1002/hipo.20202. PubMed PMID: 16921501.
1211 130. Fenton AA, Kao HY, Neymotin SA, Olypher A, Vayntrub Y, Lytton WW, et al. Unmasking
1212 the CA1 ensemble place code by exposures to small and large environments: more place cells
1213 and multiple, irregularly arranged, and expanded place fields in the larger space. J Neurosci.
1214 2008;28(44):11250-62. doi: 10.1523/JNEUROSCI.2862-08.2008. PubMed PMID: 18971467;
1215 PubMed Central PMCID: PMCPMC2695947.

1216 131. Markus EJ, Barnes CA, McNaughton BL, Gladden VL, Skaggs WE. Spatial information
1217 content and reliability of hippocampal CA1 neurons: effects of visual input. Hippocampus.
1218 1994;4(4):410-21. doi: 10.1002/hipo.450040404. PubMed PMID: 7874233.
1219

Table 1. Comparison of place cell findings in previous studies in mice and rats

Study	**Method**	**Species**	**Task**	**% place cells**	**How place cells were determined**
[97] Guzowski et al. 1999	IEG	Rat	Cylinder and platform exploration	**38-39%**	ARC detection
[98] Witharana et al. 2016	IEG	Rat	Environmental exposure and circular track	**22-73%,** mean 33±18%	Homer1a and ARC detection
[128] Talbot et al. 2018	Ephys	Mouse	Open field	**47.8%**	overall discharge rate was 0.1-2 AP/s, the spatial coherence was >0.4, and the information content was >0.4 bits/spike
[83] Jun et al. 2020	Ephys	Mouse	Open field and linear track	**50%**	Mutual information >95% of shuffled data
[129] Maurer et al. 2006	Ephys	Rat	Circular track	**~43%** on smaller track **~68%** on larger track	place field has a single cycle (360%) phase precession
[86] Wirtshafter and Wilson 2020	Ephys	Rat	Double sided T maze	**75.2%** exceeded 0.8 bits/spike **63%** had at least one place field and exceeded bits/spike threshold	1) Bits/second >0.8 2) firing in a region must be greater than two standard deviations greater than the mean firing rate and place field area must be at least 15 cm long
[130] Fenton et al. 2008	Ephys	Rat	Forage for food in cylinder and chamber	**64%** in smaller cylinder **72%** in 6x larger chamber	cell coherence was >0.25 and information content was >0.5 bits/AP, and if the cell had at least one place field.
[131] Markus et al. 1994	Ephys	Rat	8 arm radial maze forced choice	**37%**	Bits/spike cutoff of 2.29
[84] Rich et al. 2014	Ephys	Rat	48m long track	**65%** at 48m (range 46-77%)	A place field was defined as >=15 contiguous cm of rate

					map in where firing rate > 2 Hz.
[82] Meshulam et al. 2017	2p calcium imaging	Mouse	VR linear track	**~30%,** range 28% to 41%.	Mutual information above 80% of shuffled
[14] Ziv et al. 2013	1p calcium imaging	mouse	Linear track	**20%**	Mutual information above 95% of shuffled
[28] Stefanini et al. 2020	1p calcium imaging	mouse	Open field	MI mean+3σ: **~4%** for all cells **~10%** with 0.1ev/s cutoff >95% shuffled MI **~12%** for all cells **~22%** with 0.1ev/s cutoff	Mutual information > mean+3σ of the shuffled distribution. Also compared to mutual information above 95% of shuffled
[78] Kinsky et al. 2018	1p calcium imaging	mouse	Square and octagon tracks	Unspecified	1) had >= 5 calcium transients during the session 2) Mutual information above 95% of shuffled
[12] Kinsky et al. 2020	1p calcium imaging	mouse	Continuous alternation	Unspecified	1) had >= 5 calcium transients during the session 2) Mutual information above 95% of shuffled
This work	1p calcium imaging	Rat	Linear track	>95% shuffled MI **77.3%** for all cells **88.3%** with 0.01ev/s cutoff MI mean+3σ: **64.3%** for all cells **73.4%** with 0.01ev/s cutoff	Mutual information above 95% of shuffled Also computed mutual information > mean+3σ of the shuffled distribution.

Figure 1

A

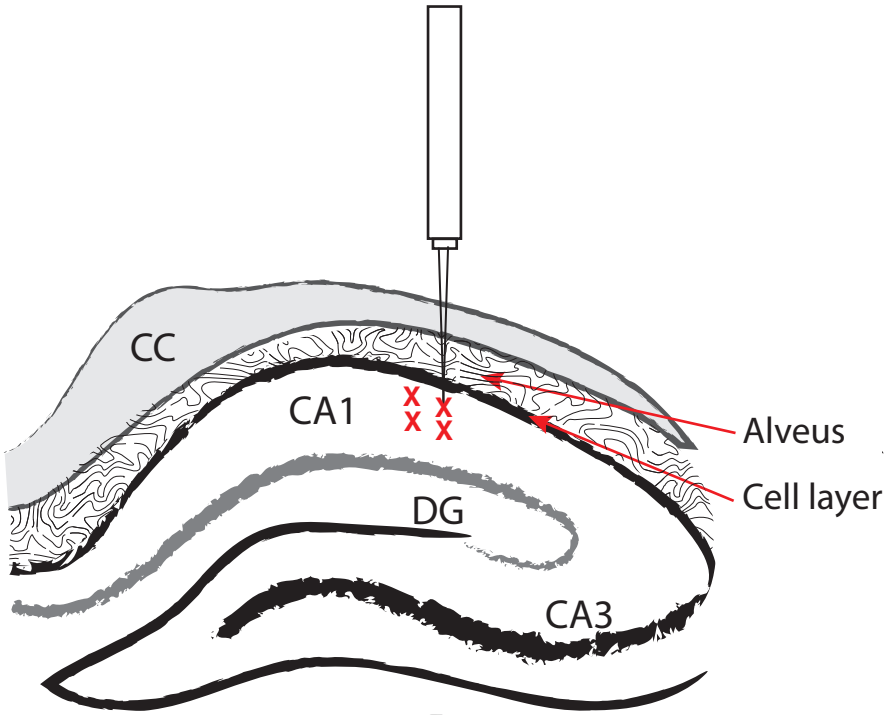
CC
CA1
DG
CA3
Alveus
Cell layer

B

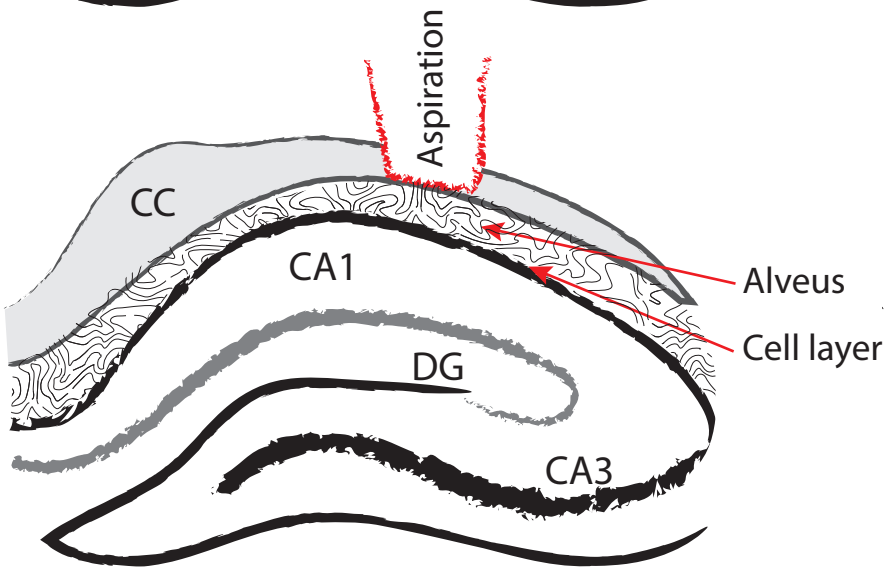
Aspiration
CC
CA1
DG
CA3
Alveus
Cell layer

C

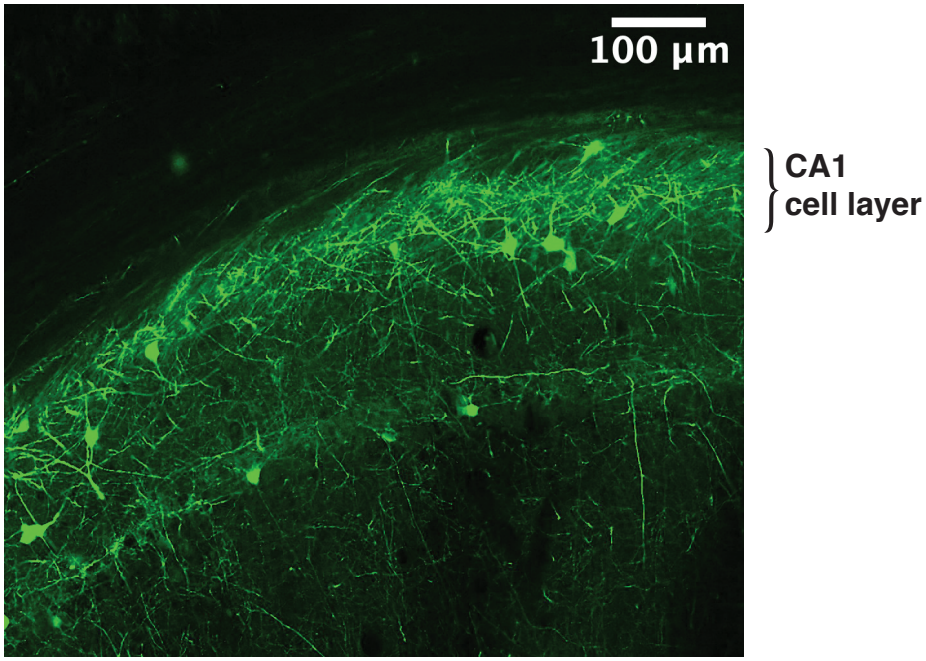
100 µm
CA1
cell layer

Figure 2

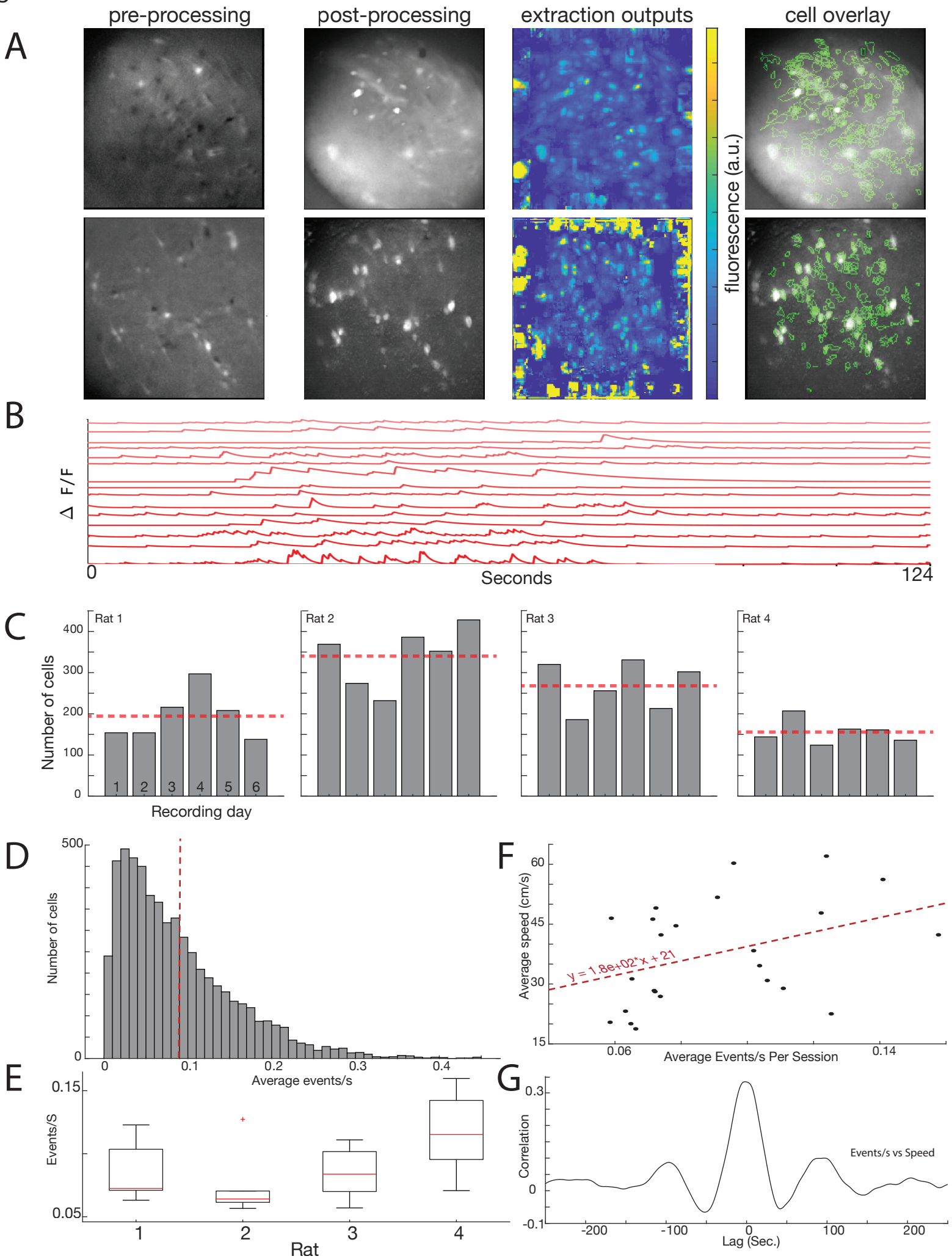
A
pre-processing
post-processing
extraction outputs
cell overlay
fluorescence (a.u.)
B
Δ F/F
0
Seconds
124
C
Rat 1
Rat 2
Rat 3
Rat 4
Number of cells
400
300
200
100
0
1
2
3
4
5
6
Recording day
D
500
Number of cells
0
0
0.1
0.2
0.3
0.4
Average events/s
E
0.15
0.05
Events/S
1
2
3
4
Rat
F
60
45
30
15
Average speed (cm/s)
y = 1.8e+02*x + 21
0.06
0.14
Average Events/s Per Session
G
0.3
0
-0.1
Correlation
Events/s vs Speed
-200
-100
0
100
200
Lag (Sec.)

Figure 3

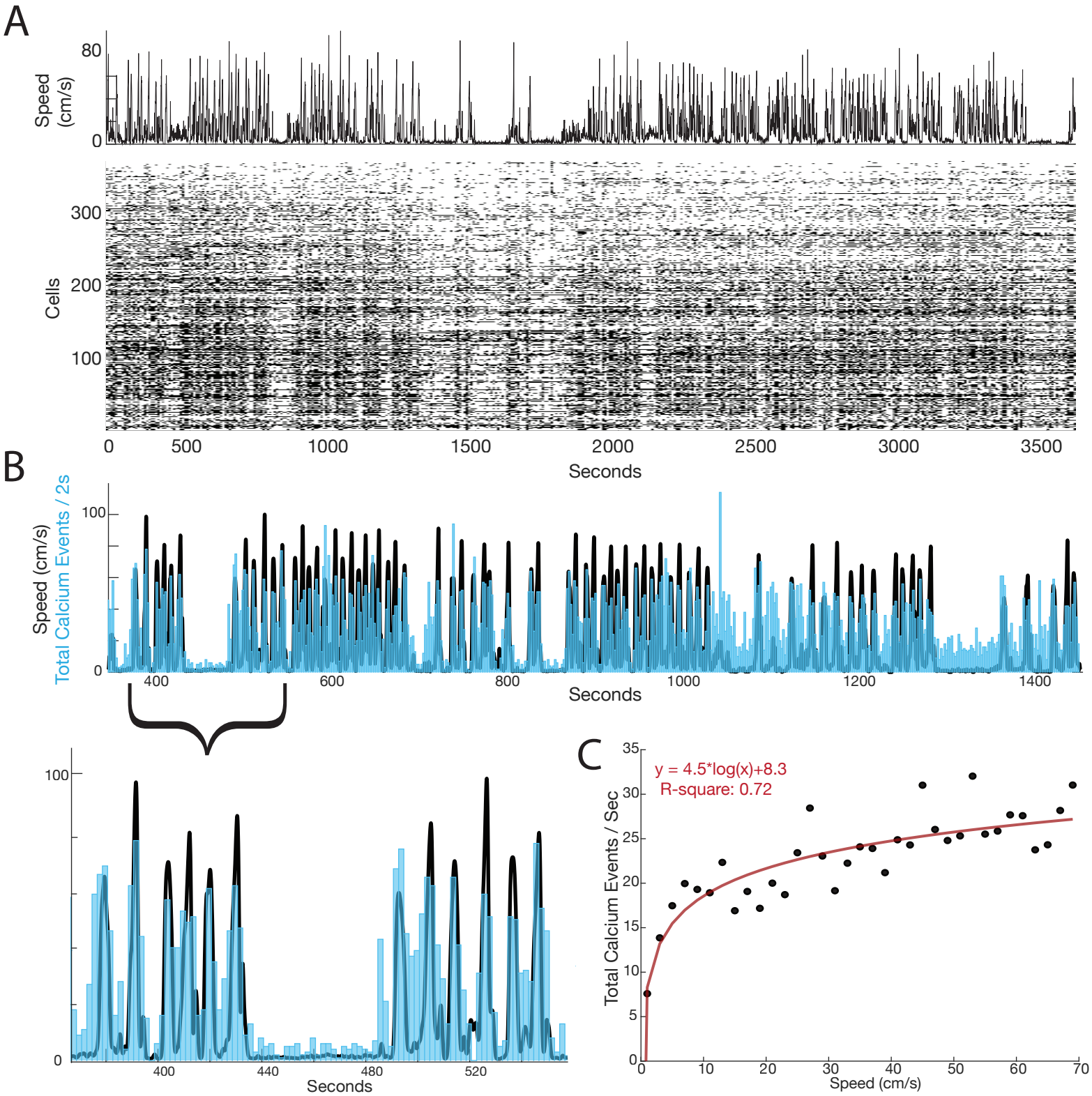
A
Speed (cm/s)
80
0
Cells
300
200
100
0
500
1000
1500
2000
2500
3000
3500
Seconds
B
Speed (cm/s)
Total Calcium Events / 2s
100
0
400
600
800
1000
1200
1400
Seconds
100
0
400
440
480
520
Seconds
C
y = 4.5*log(x)+8.3
R-square: 0.72
Total Calcium Events / Sec
35
30
25
20
15
10
5
0
0
10
20
30
40
50
60
70
Speed (cm/s)

Figure 4

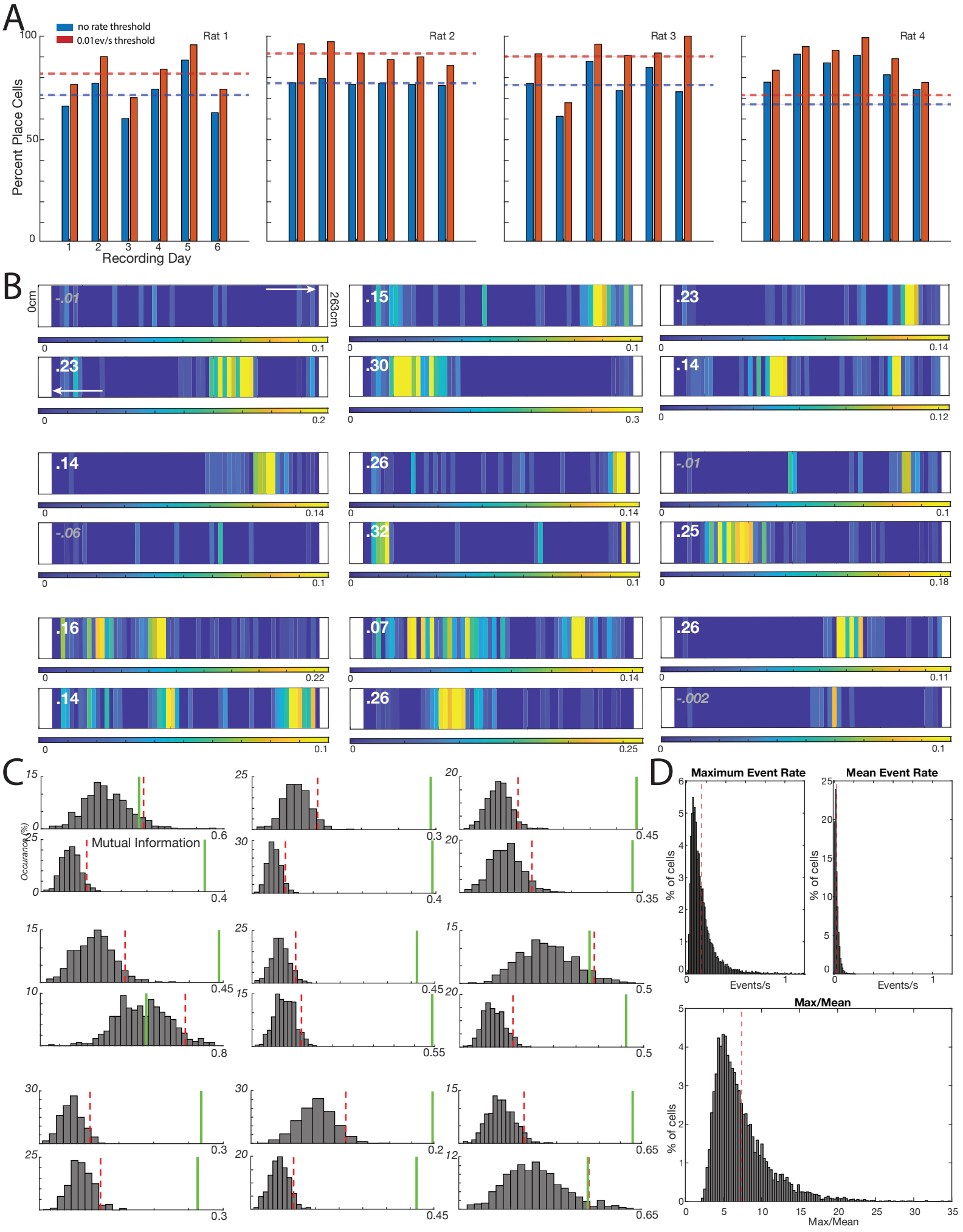
A
no rate threshold
0.01ev/s threshold
Rat 1
Rat 2
Rat 3
Rat 4
Percent Place Cells
Recording Day
B
0cm
263cm
C
Mutual Information
Occurance (%)
D
Maximum Event Rate
Mean Event Rate
% of cells
Events/s
Max/Mean

Figure 5

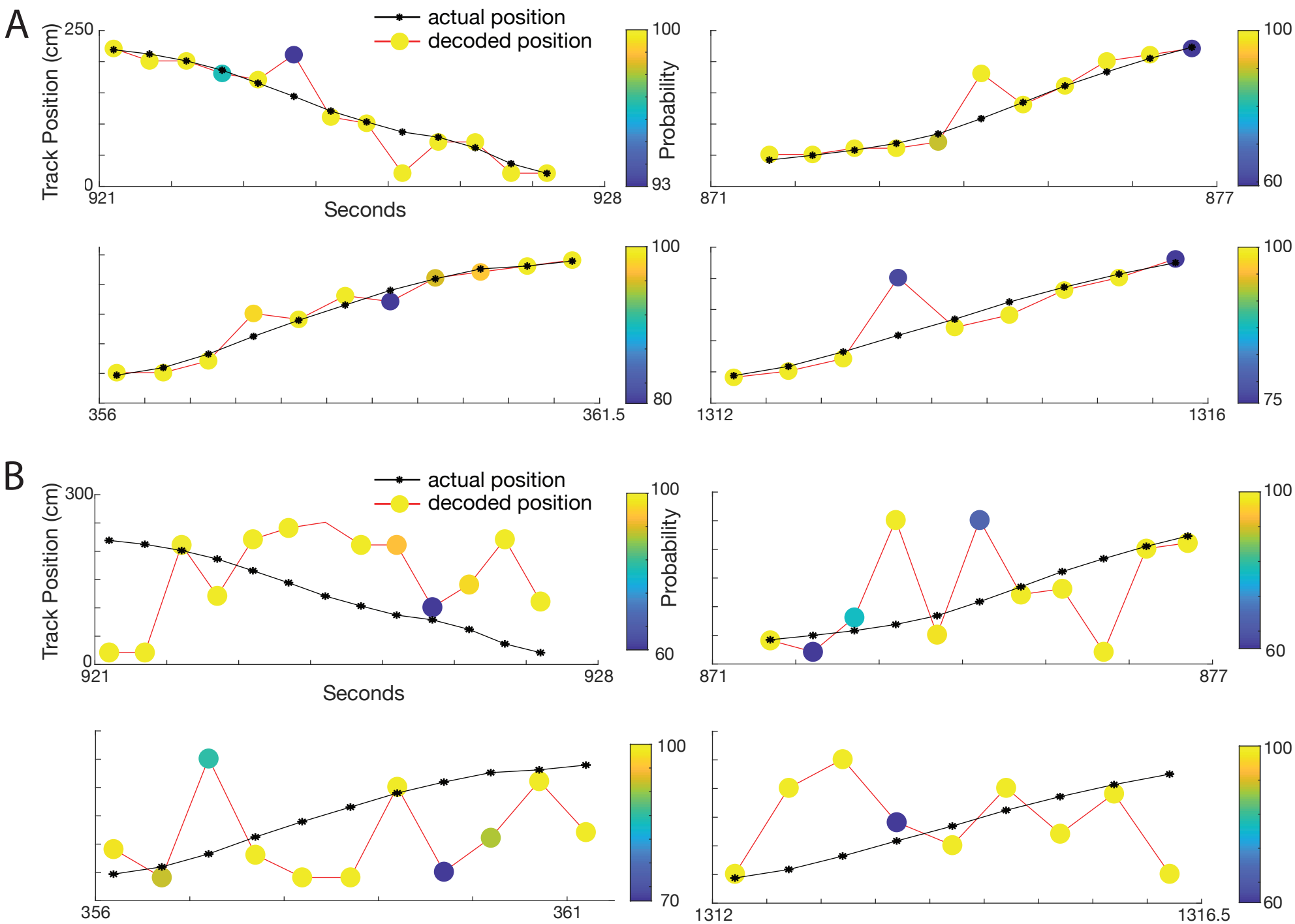
A
actual position
decoded position
Track Position (cm)
250
0
921
928
Seconds
Probability
100
93
871
877
100
60
356
361.5
100
80
1312
1316
100
75
B
actual position
decoded position
Track Position (cm)
300
0
921
928
Seconds
Probability
100
60
871
877
100
60
356
361
100
70
1312
1316.5
100
60

Figure 6

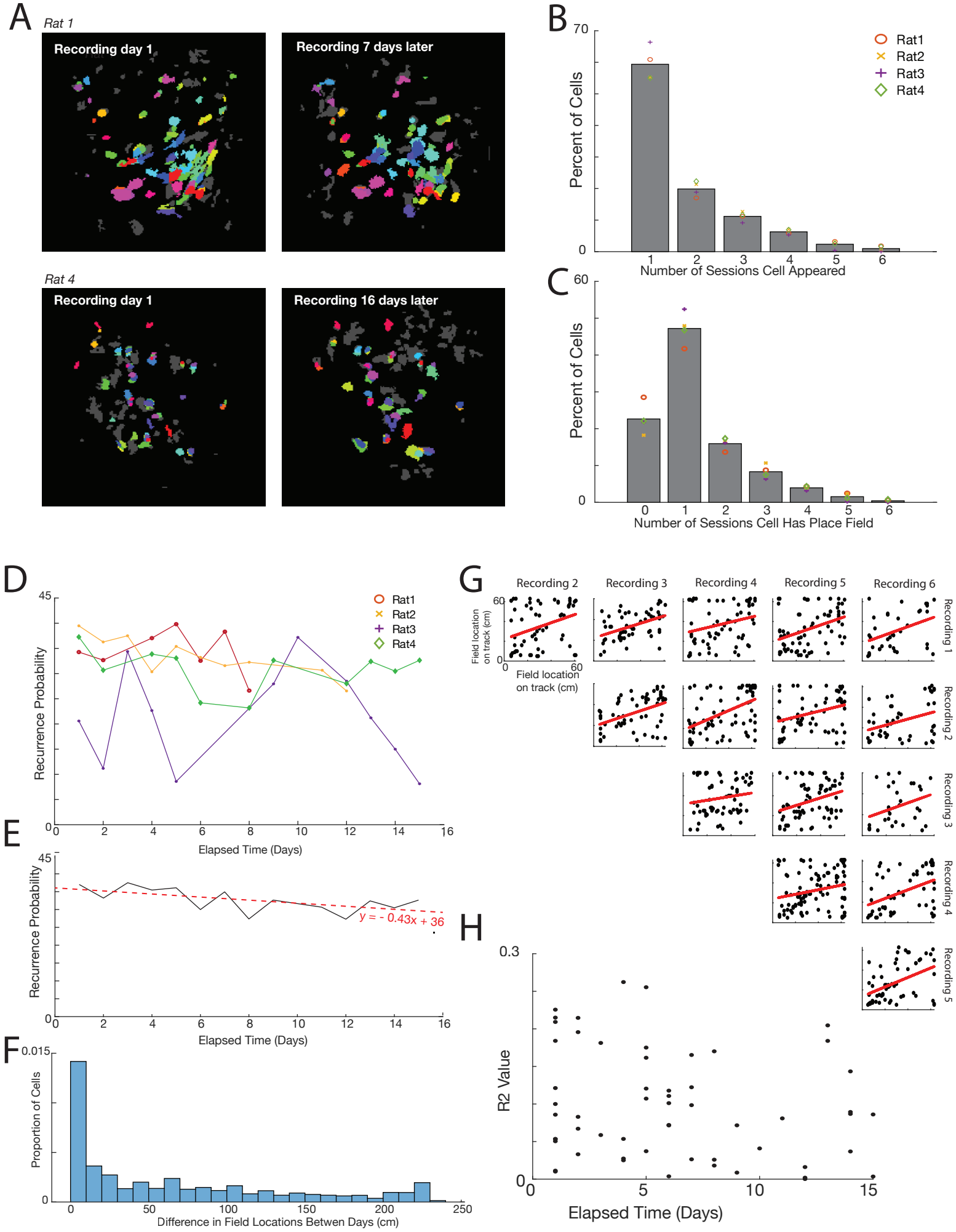
A
Rat 1
Recording day 1
Recording 7 days later
Rat 4
Recording day 1
Recording 16 days later
B
Percent of Cells
Number of Sessions Cell Appeared
Rat1
Rat2
Rat3
Rat4
C
Percent of Cells
Number of Sessions Cell Has Place Field
D
Recurrence Probability
Elapsed Time (Days)
Rat1
Rat2
Rat3
Rat4
E
Recurrence Probability
Elapsed Time (Days)
y = - 0.43x + 36
F
Proportion of Cells
Difference in Field Locations Betwen Days (cm)
G
Recording 2
Recording 3
Recording 4
Recording 5
Recording 6
Recording 1
Recording 2
Recording 3
Recording 4
Recording 5
Field location on track (cm)
Field location on track (cm)
H
R2 Value
Elapsed Time (Days)

Figure S1

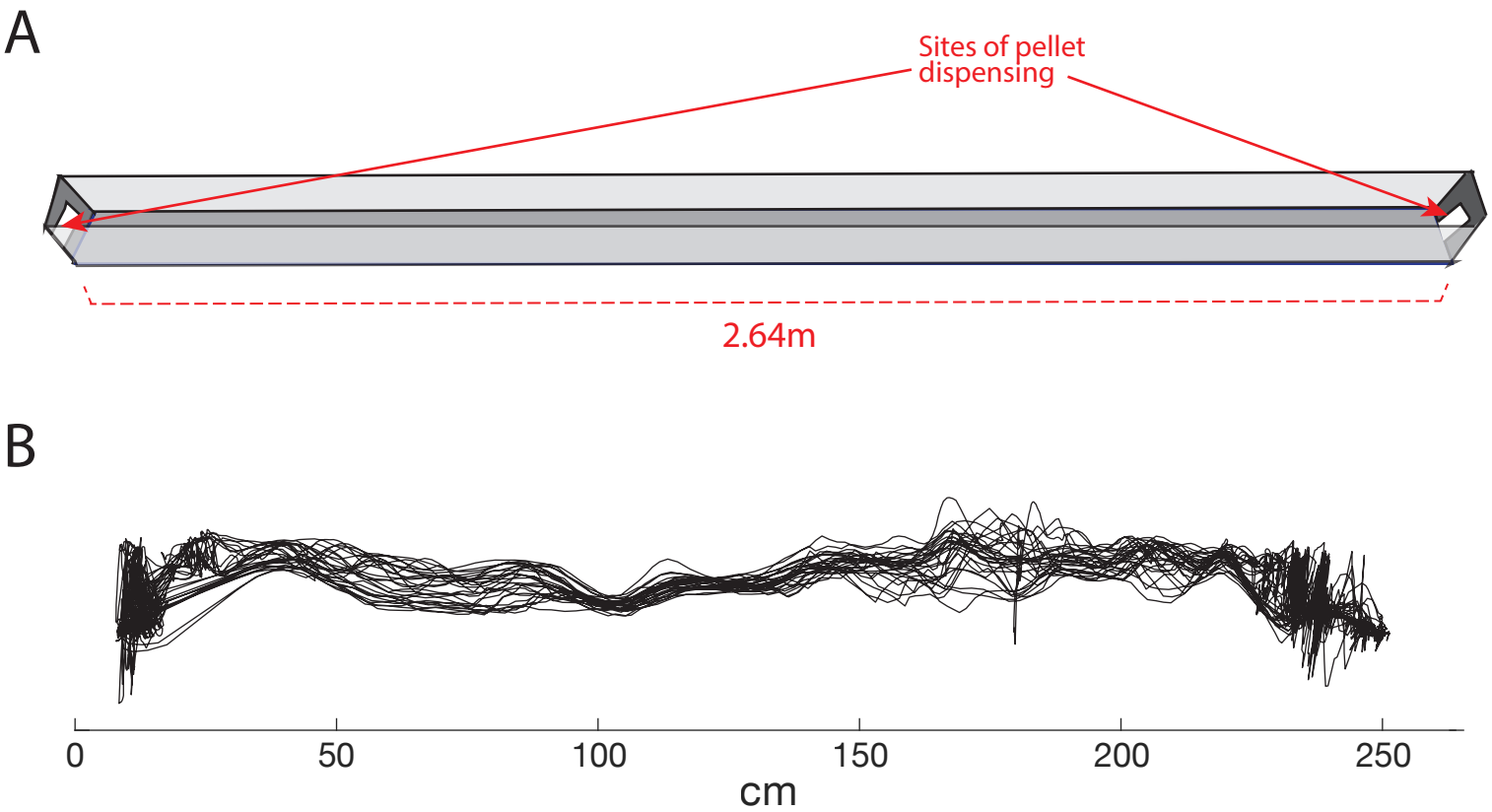

Figure S2

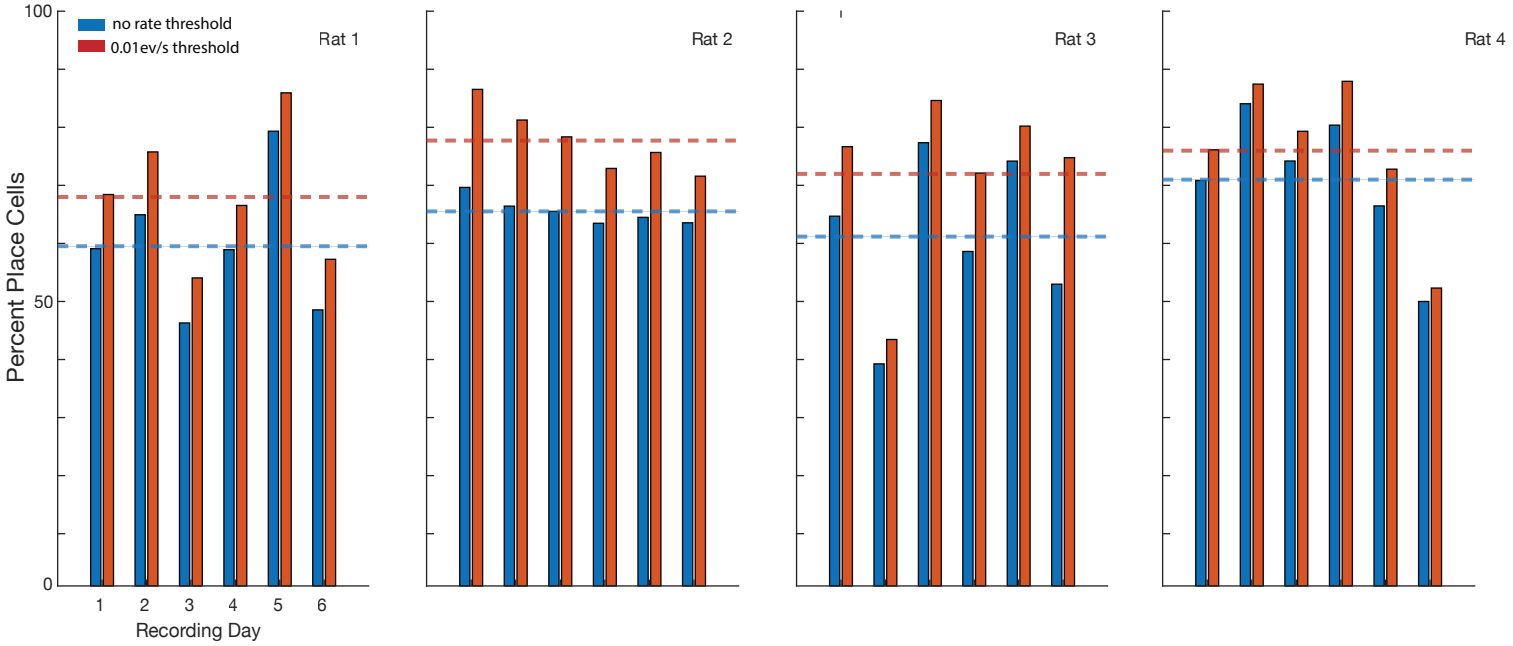
no rate threshold
0.01ev/s threshold
Rat 1
Rat 2
Rat 3
Rat 4
Percent Place Cells
100
50
0
1
2
3
4
5
6
Recording Day